New 1,2,3-triazoles and their oxime derivatives: AChE/BChE enzyme inhibitory and DNA binding properties

Ozge Gungor, Yunus Emre Veziroglu, Aysegul Kose, Seyit Ali Gungor & Muhammet Kose

	View supplementary material
	Published online: 12 Dec 2023.
	Submit your article to this journal
	Article views: 61
	View related articles
	View Crossmark data

Check for updates

New 1,2,3-triazoles and their oxime derivatives: AChE/BChE enzyme inhibitory and DNA binding properties

Ozge Gungor[a], Yunus Emre Veziroglu[a], Aysegul Kose[b], Seyit Ali Gungor[a] (iD) and Muhammet Kose[a]

[a]Chemistry Department, Kahramanmaras Sutcu Imam University, Kahramanmaras, Türkiye; [b]Department of Property Protection and Safety, Elbistan Vocational School, Istiklal University, Kahramanmaras, Türkiye

Communicated by Ramaswamy H. Sarma

ABSTRACT

1,2,3-Triazole compounds (**1a–3a**) and their oxime derivatives (**1b–3b**) were synthesized. The structures of these synthesized compounds were characterized using common spectroscopic methods. Crystal structures of the compounds **3, 2b** and **3b** were determined by single crystal X-ray diffraction studies. The acetylcholinesteras (AChE) and butyrylcholinesterase (BChE) cholinesterase inhibitor (ChEI) and DNA/calf serum albumin (BSA) binding properties of the compounds were examined. DNA binding studies have shown that compounds interact with DNA through 1,2,3-triazole and oxime groups. When the binding constant K_b values were compared, it was revealed that compound **3b** ($K_b = 4.6 \times 10^5 \ M^{-1}$) with oxime in its structure binds more strongly than the others. In addition, in vitro BSA binding studies showed that compounds **1b** and **3b** exhibited higher binding affinity. These results confirm that the quenching is due to the formation of a compound resulting from the static quenching mechanism, rather than being initiated by a dynamic mechanism. Likewise, when the enzyme activity of the compounds was examined, the compounds exhibited high inhibitory activity against AChE. The highest activity was observed for compounds **2b** and **3b** (8.6 ± 0.05 and $4.8 \pm 0.052 \ \mu M$). It was observed that the compounds were not selective with respect to BChE. Communicated by Ramaswamy H. Sarma

Abbreviation: AD: Alzheimer's disease; AChE: Acetylcholinesteras; BChE: Butyrylcholinesterase; DNA: Deoxyribose nucleic acid; BSA: Calf serum albumin; ChEIs: Cholinesterase inhibitors; THF: Tetrahydrofuran; FT-IR: Fourier Transform Infrared Spectroscopy; T.L.C.: Thin layer chromatography; DMSO: Dimethylsulfoxide; DMF: Dimethylformamide; ACh: Acetylcholine; FDA: Food and Drug Administration; IC_{50}: Half-maximum inhibitory concentrations; [S]: Concentrations of substrate; Ki: Inhibitor constant; K_{sv}: Dynamic quenching constant; K_q: Quenching rate constant of BSA; ΔG: Gibbs Free Energy change; ΔH: Enthalpy change; ΔS: Entropy change; FSdsDNA: Fish sperm DNA; K_b: Binding constant; K_{app}: association constants; n: Binding site number; EB: Ethidium bromide; GNT: Galantamine; THA: Tacrine; NPS: (2S)-2-(6-methoxynaphthalen-2-yl)propanoic acid; HT: 2'-(4-hydroxyphenyl)-5-(4-methyl-1-piperazinyl)-2,5'-bi-benzimidazole; RMSD: Root mean square error

1. Introduction

Scientists have made significant efforts to synthesize and develop a large number of bioactive compounds due to their importance to societies and the humanities. 1,2,3-Triazoles have shown fascinating pharmaceutical applications (Abdel-Wahab et al., 2012). The three nitrogen atoms in the triazole ring make it easy to bind to a variety of enzymes and biological receptors via different interactions (weak interactions like hydrogen interactions, Van der Waal interactions, dipole–dipole interactions and hydrophobic interactions). Because of these properties, they have exhibited chemotherapeutic properties such as antiprotozoals with broad biological properties (Yadav et al., 2017), anti-HIV (Pala et al., 2016) antimicrobial (Yadav et al., 2017) and anti-tuberculosis

(Venugopala et al., 2016), Alzheimer's, choline esterase inhibitors (Najafi et al., 2017) and anticancer activities (Li et al., 2011). In addition, 1,2,3-triazoles have received great attention due to their potential applications in supramolecular chemistry and organometallic chemistry and medicinal chemistry. Oxime-containing molecules have become to our attention because they appear to be amenable to biotransformation (Botta et al., 2011). Due to their ability to transfer acyl groups, these classes of compounds have recently become important in the synthesis of new drug candidates for the treatment of various diseases and in the design and development of new therapeutic agents. For example, furan oximes were found to inhibit DNA (Abele & Lukevics, 2010; Botta et al., 2011), lipid leukaemia cells: RNA

Bu belge güvenli Elektronik İmza ile imzalanmıştır.
Evrak sorgulaması https://turkiye.gov.tr/ebd?eK=5637&eD=BSDNTKR88J&eS=40446 adresinden yapılabilir.

and protein synthesis. Quinoline oxime derivatives also have antitumour activity. The photodynamic therapy of prostate tumours has also been monitored with hexamethylpropylen-amine oxime derivatives (Abele et al., 2005).

The basic composition of living organisms is deoxyribo-nucleic acid and many biochemical processes in the cellular system are regulated by the biomolecule DNA (Rakesh et al., 2019). Therefore, understanding and studying the interactions of biological targets with nucleic acids and how they interact can provide more confident insights at the molecular level and is very important for the development of new drugs in the biological field (Knappe et al., 2023; Pala et al., 2016; Weng et al., 2020). The aim is to design different compounds that are able to bind to DNA (between nucleotides or between strands), to cleave DNA and to interact with certain proteins, which are the main cellular targets of anti-cancer derivatives. Investigation of the interactions of synthesized molecules with calf serum albumin (BSA) by spectroscopic methods provides important information about a determined binding mode or interactions (Tian et al., 2010).

The most important therapeutic effect of cholinesterase inhibitors (ChEIs) used to treat Alzheimer's disease (AD) is to stabilise cognitive function for at least one year in about 50% of patients (Kumar et al., 2020; Vecchio et al., 2021). Recent evidences have revealed that both acetylcholinester-ase (AChE) and butyrylcholinesterase (BuChE) play a role in the breakdown of ACh in the brain, and that inhibiting both enzymes could increase the effectiveness of treatment and expand the indications (Gungor & Kose, 2023).

Here, we synthesized a new 1,2,3-triazole and 1,2,3-tri-azole oxime derivatives and screened for their cholinesterase enzyme inhibitory properties (Figure 1). The structures of the new compounds were determined first, followed by DNA/BSA binding studies and cholinesterase enzyme inhibition activity. Finally, molecular docking studies were carried out for the synthesized compounds in order to establish the binding mechanisms.

2. Experimental

2.1. General methods

All starting materials and organic solvents were purchased from commercial sources and used as received without further purification. FT-IR spectra of the compounds were performed on a Perkin Elmer Paragon 1000 PC. ^{1}H and ^{13}C NMR spectra in dimethylsulfoxide (DMSO)-d_6 were recorded on a Bruker 400 MHz instrument and TMS was used as an internal standard.

2.2. Synthesis of 2-oxo-propargyl-benzaldehyde derivatives (1–3)

Salicylaldehyde, 3-methoxy salicylaldehyde or 3-ethoxy salicylaldehyde (5 mmol) were dissolved in acetonitrile (25 mL). To the reaction solutions, K_2CO_3 (11 mmol) was added and then stirred at room temperature for half an hour. Propargyl bromide (5.5 mmol) was then added to the reactions and the stirring was continued for 48 h. The progress of the reactions was followed by thin layer chromatography (T.L.C). Upon completion of the reactions, the solvent was removed on a rotary evaporator. The crude products suspended in water (30 mL) were extracted with ethyl acetate (3 × 25 mL). The organic layers were combined and dried on Na_2SO_4. The solvent was removed on a rotary evaporator to give pure 2-oxo-propargyl-benzaldehyde derivatives (1–3).

2.2.1. 2-(Prop-2-yn-1-yloxy)benzaldehyde (1)

Chemical formula: $C_{10}H_8O_2$. Molecular weight: 160.05 g/mol. Colour: Light yellow crystals. Yield: 71.25%. M.p.: 55–60 °C. Elemental analysis Calc. for $C_{10}H_8O_2$: C, 74.99; H, 5.03. Found: C, 74.83; H, 4.92. ^{1}H NMR (400 MHz, CDCl$_3$, ppm) δ 10.52(1H, s, CH=O), 7.89(1H, d, CH$_{phenyl}$), 7.60(1H, d, CH$_{phenyl}$), 7.10(2H, t, CH$_{phenyl}$), 4.86(2H, s, -OCH$_2$-), 2.61(1H, s, C≡CH). ^{13}C NMR (101 MHz, CDCl$_3$, ppm) δ189.57($\underline{C}$H=O), 159.74(C$_{phenyl}$), 135.79(C$_{phenyl}$), 128.52(C$_{phenyl}$), 125.39(C$_{phenyl}$), 121.66(C$_{phenyl}$),

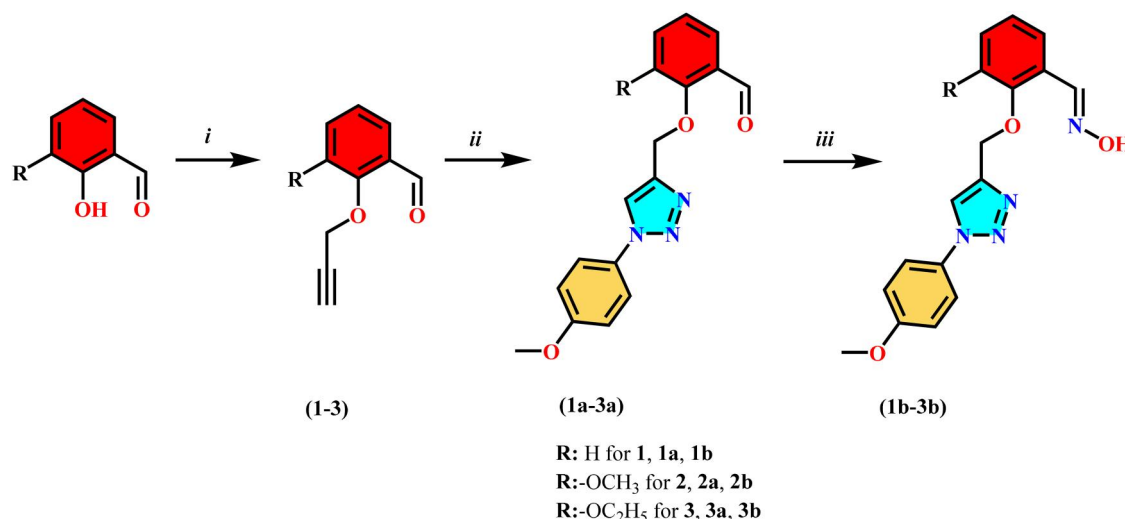**Figure 1.** Synthesis reactions of 1,2,3-triazole-oxime derivatives. (i) Propargyl bromide, K_2CO_3, acetonitrile. (ii) CuSO$_4$.5H$_2$O, sodium ascorbate, THF/H$_2$O. (iii) Hydroxylamine hydrochloride, NaOAc.

R: H for **1, 1a, 1b**
R: -OCH$_3$ for **2, 2a, 2b**
R: -OC$_2$H$_5$ for **3, 3a, 3b**

113.19(C_{phenyl}), 77.69(-C≡CH), 76.58(-C≡CH), 56.35(OCH_2-). FTIR (cm^{-1}, ATR): 3269, 2973, 2873, 2116, 1679, 1662, 1595, 1480, 1455, 1398, 1285, 1262, 1220, 1192, 1165, 1104, 1044, 1005, 924, 831, 755, 674, 653, 610, 547, 526, 461, 442.

2.2.2. 3-Methoxy-2-(prop-2-yn-1-yloxy)benzaldehyde (2)

Chemical formula: $C_{11}H_{10}O_3$. Molecular weight: 190.20 g/mol. Colour: Light yellow crystals. Yield: 69.4%. M.p.: 45–50 °C. Elemental analysis Calc. for $C_{11}H_{10}O_3$: C, 69.46; H, 5.30. Found: C, 69.31; H, 5.16. ^{1}H NMR (400 MHz, CDCl$_3$, ppm) δ 10.50(1H, s, CH=O), 7.47(1H, t, CH$_{phenyl}$), 7.19(2H, d, CH$_{phenyl}$), 4.89(2H, s, -OCH$_2$-), 3.91(3H, s, -OCH$_3$), 2.49(1H, s, C≡CH). ^{13}C NMR (101 MHz, CDCl$_3$, ppm) δ 190.52(CH=O), 152.80(C_{phenyl}), 149.39(C_{phenyl}), 131.03(C_{phenyl}), 124.92(C_{phenyl}), 118.68(C_{phenyl}), 117.74(C_{phenyl}), 78.29(-C≡CH), 77.02(-C≡CH), 60.79(OCH_2-), 55.98(OCH_3). FTIR (cm^{-1}, ATR): 3266, 2936, 2890, 2838, 2118, 1682, 1595, 1583, 1477, 1437, 1383, 1317, 1249, 1201, 1178, 1066, 981, 911, 781, 748, 665, 649, 602, 529, 516, 483.

2.2.3. 3-Ethoxy-2-(prop-2-yn-1-yloxy)benzaldehyde (3)

Chemical formula: $C_{12}H_{12}O_3$. Molecular weight: 204.23 g/mol. Colour: Light yellow crystals. Yield: 90.10%. M.p.: 65–70 °C. Elemental analysis Calc. for $C_{12}H_{12}O_3$: C, 70.58; H, 5.92. Found: C, 70.39; H, 5.78. ^{1}H NMR (400 MHz, CDCl$_3$, ppm) δ 10.50(1H, s, CH=O), 7.45(1H, t, CH$_{phenyl}$), 7.15(2H, d, CH$_{phenyl}$), 4.92(2H, s, -OCH$_2$-), 4.14(2H, q, -OCH$_2$CH$_3$), 2.50(1H, s, C≡CH), 1.48(3H, t, -OCH$_2$CH$_3$). ^{13}C NMR (101 MHz, CDCl$_3$, ppm) δ 190.61(CH=O), 152.10(C_{phenyl}), 149.57(C_{phenyl}), 131.05(C_{phenyl}), 124.81(C_{phenyl}), 118.71(C_{phenyl}), 118.59(C_{phenyl}), 78.36(-C≡CH), 76.89(-C≡CH), 64.56(OCH_2-), 60.66(OCH_2CH$_3$), 14.78(OCH_2CH$_3$). FTIR (cm^{-1}, ATR): 3259, 2975, 2932, 2890, 2112, 1683, 1584, 1481, 1469, 1393, 1315, 1247, 1192, 1112, 1081, 1057, 949, 969, 915, 867, 785, 765, 751, 685, 667, 604, 558, 515, 493.

2.3. Synthesis of 1,2,3-triazole-aldeyhde derivatives (1a–3a)

1,2,3-Triazole derivatives (**1a–3a**) were synthesized according to the reported procedure (Çot et al., 2023; Güngör et al., 2022). Compounds **1–3** (3 mmol) were dissolved in tetrahydrofuran (THF)/H$_2$O (15/5 mL) and followed by addition of CuSO$_4$.5H$_2$O (0.6 mmol) and sodium ascorbate (1.2 mmol). The resulting reaction mixtures were stirred at room temperature for 15 min and then 4-methoxy-phenylazide (3.9 mmol) was added. The resulting reaction mixtures were further stirred at room temperature for 24 h. Upon completion of the reactions, solvent was removed to give sticky products. These were dissolved in water (20 mL) and extracted with ethyl acetate (3 × 30 mL). Organic fragments were collected and dried on Na$_2$SO$_4$. Pure 1,2,3-triazole compounds were obtained upon removal of the solvent on a rotary evaporator.

2.3.1. 2-((1-(4-Methoxyphenyl)-1H-1,2,3-triazol-4-yl)methoxy)benzaldehyde (1a)

Chemical formula: $C_{17}H_{15}N_3O_3$. Molecular weight: 309.33 g/mol. Colour: Orange powder. Yield: 37.76%. M.p.: 120–125 °C. Elemental analysis Calc. for $C_{17}H_{15}N_3O_3$: C, 66.01; H, 4.89; N, 13.58. Found: C, 69.82; H, 4.77; N, 13.43. ^{1}H NMR (400 MHz, CDCl$_3$, ppm) δ10.51(1H, s, CH=O), 8.05(1H, s, CH$_{triazole}$), 7.87–7.03(8H, m, CH$_{phenyl}$), 5.43(2H, s, -OCH$_2$-), 3.88(3H, s, -OCH$_3$). ^{13}C NMR (101 MHz, CDCl$_3$, ppm) δ189.62(CH=O), 160.43(C_{phenyl}), 159.98(C_{phenyl}), 143.83($C_{triazole}$), 136.08(C_{phenyl}), 130.23(C_{phenyl}), 128.75, 125.05(C_{phenyl}), 122.24(C_{phenyl}), 121.64(C_{phenyl}), 121.37(C_{phenyl}), 114.82($C_{triazole}$), 113.01(C_{phenyl}), 62.48(OCH_2-), 55.65(OCH_3). FTIR (cm^{-1}, ATR): 3152, 3066, 2923, 1682, 1597, 1519, 1485, 1454, 1403, 1288, 1246, 1233, 1186, 1157, 1100, 1045, 988, 823, 758, 613, 519.

2.3.2. 3-Methoxy-2-((1-(4-methoxyphenyl)-1H-1,2,3-triazol-4-yl)methoxy)benzaldehyde (2a)

Chemical formula: $C_{18}H_{17}N_3O_4$. Molecular weight: 339.35 g/mol. Colour: Orange powder. Yield: 37.45%. M.p.: 105–110 °C. Elemental analysis Calc. for $C_{18}H_{17}N_3O_4$: C, 63.71; H, 5.05; N, 12.38. Found: C, 63.5; 5H, 4.83; N, 12.16. ^{1}H NMR (400 MHz, CDCl$_3$, ppm) δ 10.35(1H, s, CH=O), 7.98(1H, s, CH$_{triazole}$), 7.64–7.03(7H, m, CH$_{phenyl}$), 5.44(2H, s, -OCH$_2$-), 3.98(3H, s, -OCH$_3$), 3.89(3H, s, -OCH$_3$). ^{13}C NMR (101 MHz, CDCl$_3$, ppm) δ 190.25(CH=O), 159.92(C_{phenyl}), 152.92($C_{triazole}$), 150.32(C_{phenyl}), 130.14(C_{phenyl}), 124.65(C_{phenyl}), 122.32(C_{phenyl}), 119.26(C_{phenyl}), 118.04(C_{phenyl}), 114.78($C_{triazole}$), 67.07(OCH_2-), 56.12(OCH_3), 55.64(OCH_3). FTIR (cm^{-1}, ATR): 3150, 2888, 1683, 1582, 1520, 1482, 1452, 1376, 1343, 1305, 1245, 1215, 1182, 1112, 1064, 1049, 1032, 963, 908, 858, 828, 772, 760, 737, 696, 651, 610, 574, 531.

2.3.3. 3-Ethoxy-2-((1-(4-methoxyphenyl)-1H-1,2,3-triazol-4-yl)methoxy)benzaldehyde (3a)

Chemical formula: $C_{19}H_{19}N_3O_4$. Molecular weight: 353.38 g/mol. Colour: Orange-red. Yield: 50.30%. M.p.: 105–110 °C. Elemental analysis Calc. for $C_{19}H_{19}N_3O_4$: C, 64.58; H, 5.42; N, 11.89. Found: C, 64.45; H, 5.31; N, 11.68. ^{1}H NMR (400 MHz, CDCl$_3$, ppm) δ 10.50(1H, s, CH=O), 7.98(1H, s, CH$_{triazole}$), 7.64–6.95(7H, m, CH$_{phenyl}$), 5.46(2H, s, -OCH$_2$-), 4.19(2H, q, -OCH$_2$CH$_3$), 3.87(3H, s, -OCH$_3$), 1.54(3H, t, -OCH$_2$CH$_3$). ^{13}C NMR (101 MHz, CDCl$_3$, ppm) δ 190.31(CH=O), 159.83(C_{phenyl}), 152.19(C_{phenyl}), 151.74(C_{phenyl}), 150.48(C_{phenyl}), 147.47($C_{triazole}$), 135.98(C_{phenyl}), 130.08(C_{phenyl}), 124.50(C_{phenyl}), 122.22(C_{phenyl}), 119.58(C_{phenyl}), 119.17(C_{phenyl}), 114.80($C_{triazole}$), 112.81(C_{phenyl}), 65.85(OCH_2-), 64.99(-OCH$_2$CH$_3$), 55.63(-OCH$_3$), 14.90(-OCH$_2$CH$_3$). FTIR (cm^{-1}, ATR): 3158, 2977, 1683, 1583, 1520, 1483, 1471, 1396, 1377, 1320, 1244, 1216, 1190, 1113, 1059, 1047, 1032, 953, 860, 825, 801, 764, 736, 698, 660, 612, 576, 534, 522.

2.4. Synthesis of 1,2,3-triazole oxime derivatives (1b–3b)

Triazole-oxime derivatives (**1b–3b**) were prepared according to the known method (Abdel-Aziz et al., 2013). The triazole

compounds (**1a–3a**) (1 mmol) and hydroxylamine hydrochloride (4 mmol) were dissolved in absolute ethanol (25 mL). The reaction solutions were stirred for 30 min followed by addition of sodium acetate (4 mmol). The resulting reaction mixtures were refluxed for 5 h. The progress of the reactions was followed by T.L.C. The reaction mixtures were then cooled to the room temperature and poured into ice cold water (50 mL). The products were then extracted with ethyl acetate (3 × 30 mL). Organic layers were combined and dried on Na_2SO_4. Solvent was removed on a rotary evaporator to give pure 1,2,3-triazole oxime derivatives.

2.4.1. (E)-2-((1-(4-methoxyphenyl)-1H-1,2,3-triazol-4-yl)methoxy)benzaldehyde oxime (1b)

Chemical formula: $C_{17}H_{16}N_4O_3$. Molecular weight: 324.34 g/mol. Colour: Orange. Yield: 64.72%. M.p.: 135–140 °C. Elemental analysis Calc. for $C_{17}H_{16}N_4O_3$: C, 62.95; H, 4.97; N, 17.27. Found: C, 62.69; H, 4.85; N, 17.13. ^{1}H NMR (400 MHz, CDCl3, ppm) δ 8.54(1H, s, CH=N), 8.25(1H, br, OH), 8.00(1H, s, CH_triazole), 7.76–7.00(8H, m, CH_phenyl), 5.37(2H, s, -OCH_2-), 3.89(3H, s, -OCH_3). ^{13}C NMR (101 MHz, CDCl3, ppm) δ 159.97(CH=N), 156.19(C_phenyl), 146.48(C_phenyl), 144.35(C_triazole), 131.34(C_phenyl), 130.33(C_phenyl), 126.91(C_phenyl), 122.36(C_phenyl), 121.52(C_phenyl), 121.22(C_phenyl), 121.01(C_phenyl), 114.80(C_triazole), 112.63(C_phenyl), 62.53(OCH_2-), 55.65(OCH_3). FTIR (cm⁻¹, ATR): 3473, 3175, 2995, 1609, 1598, 1580, 1517, 1497, 1450, 1411, 1316, 1299, 1283, 1248, 1189, 1110, 1054, 1039, 989, 951, 892, 874, 830, 790, 747, 667, 632, 613, 580, 525, 481, 432.

2.4.2. (E)-3-methoxy-2-((1-(4-methoxyphenyl)-1H-1,2,3-triazol-4-yl)methoxy)benzaldehyde oxime (2b)

Chemical formula: $C_{18}H_{18}N_4O_4$. Molecular weight: 354.37 g/mol. Colour: Orange-yellow. Yield: 66.90%. M.p.: 140–145 °C. Elemental analysis Calc. for $C_{18}H_{18}N_4O_4$: C, 61.01; H, 5.12; N, 15.81. Found: C, 69.83; H, 5.02; N, 15.68. ^{1}H NMR (400 MHz, CDCl3, ppm) δ 8.44(1H, s, CH=N), 8.28(1H, br, OH), 8.00(1H, s, CH_triazole), 7.65–6.97(7H, m, CH_phenyl), 5.31(2H, s, -OCH_2-), 3.93(3H, s, -OCH_3), 3.87(3H, s, -OCH_3). ^{13}C NMR (101 MHz, CDCl3, ppm) δ159.86(CH=N), 152.85(C_phenyl), 146.23(C_phenyl), 145.87(C_phenyl), 144.64(C_triazole), 126.57(C_phenyl), 126.47(C_phenyl), 124.79(C_phenyl), 122.43(C_phenyl), 121.62(C_phenyl), 118.04(C_phenyl), 114.76(C_triazole), 113.51(C_phenyl), 66.68(OCH_2-), 55.89(OCH_3), 55.63(OCH_3. FTIR (cm⁻¹, ATR): 3170, 2917, 1610, 1572, 1517, 1473, 1437, 1374, 1314, 1248, 1197, 1108, 1024, 967, 831, 780, 664, 641, 609, 575, 525, 465.

2.4.3. (E)-3-ethoxy-2-((1-(4-methoxyphenyl)-1H-1,2,3-triazol-4-yl)methoxy)benzaldehyde oxime (3b)

Chemical formula: $C_{19}H_{20}N_4O_4$. Molecular weight: 368.39 g/mol. Colour: Orange. Yield: 61.62%. M.p.: 145–150 °C. Elemental analysis Calc. for $C_{19}H_{20}N_4O_4$: C, 61.95; H, 5.47; N, 15.21. Found: C, 61.81; H, 5.36; N, 15.04. ^{1}H NMR (400 MHz, CDCl3, ppm) δ 8.45(1H, s, CH=N), 8.30(1H, br, OH), 7.99(1H, s, CH_triazole), 7.65–6.96(7H, m, CH_phenyl), 5.33(2H, s, -CH_2-), 4.17(2H, q, -OCH_2CH_3), 3.88(3H, s, -OCH_3), 1.51(3H, t,

-OCH_2CH_3). ^{13}C NMR (101 MHz, CDCl3, ppm) δ159.85(CH=N), 152.11(C_phenyl), 146.37(C_phenyl), 146.11(C_triazole), 130.57(C_phenyl), 126.53(C_phenyl), 124.68(C_phenyl), 122.39(C_phenyl), 121.49(C_phenyl), 119.40(C_phenyl), 118.99(C_phenyl), 117.84(C_phenyl), 114.76(C_triazole), 66.71(OCH_2-), 64.32(OCH_2CH_3), 55.63(OCH_3), 14.94(OCH_2CH_3). FTIR (cm⁻¹, ATR): 3148, 2928, 1610, 1572, 1516, 1462, 1439, 1374, 120, 1108, 1059, 1025, 955, 825, 790, 673, 635, 612, 573, 453.

2.5 X-ray structures solution and refinement for the compounds

The method for single crystal X-ray crystallographic data for compounds **3**, **2b** and **3b** is given in the supplementary section. Table S1 provides the crystal data and refining information.

2.6. Biological assays

Methods of all biological activity (DNA and BSA binding, Viscosity assay, AChE, BChE and Kinetic assay) studies are given in the supplementary section.

2.7. Molecular docking studies

The method of *in silico* studies is given in the supplementary section.

3. Results and discussion

3.1. Chemistry

Three new 1,2,3-triazole compounds (**1a–3a**) and their oxime derivatives (**1b–3b**) were prepared in two steps reactions. In the first step, the 1,2,3-triazole (**1a–3a**) compounds were synthesized by the click reaction of oxo-propargyl benzaldehydes (**1–3**) and 4-methoxyazidobenzene. The 1,2,3-triazole compounds were then reacted with hydroxyl amine to yield 1,2,3-triazole oxime derivatives (**1b–3b**). The compounds are soluble in common organic solvents such as chloroform, methanol, ethanol, THF, DMSO and dimethylformamide (DMF) and are insoluble in water. The structure of the compounds was characterized by FTIR, ^{1}H/^{13}C NMR spectroscopies. The purity of the compounds was further confirmed by elemental analysis. The experimentally obtained C, H and N values of the compounds were found to be in good agreement with the calculated values. In addition, single crystals of compounds **3**, **2b** and **3b** were obtained and the crystal structures of these compounds were determined by single crystal X-ray diffraction studies.

FTIR spectra of the compounds were performed and their characteristic stretching vibrations were determined. When the FTIR spectra of 2-oxopropargylbenzaldehyde compounds (**1–3**) are examined, the stretching vibrations observed at 2110 cm⁻¹ originate from the terminal alkyne groups v̄(C≡CH) in the compounds. In addition, stretching peaks belonging to aldehyde groups v̄(C=O) in the spectra of these compounds were observed in the range of 1670–

1680 cm^{-1}. The weak vibration peaks observed in the range of 2970–2850 cm^{-1} in the spectra of the compounds are due to aliphatic C-H stretching's. The absence of stretching vibrations of the terminal alkyne groups in the FTIR spectra of 1,2,3-triazole compounds (**1a–3a**) indicates that click reactions occur and 1,2,3-triazole compounds are formed. The bond stretching vibrations of the aldehyde groups $\bar{\upsilon}(C=O)$ in the compounds were observed as sharp peaks at approximately 1680 cm^{-1}. In addition, $\bar{\upsilon}(N=N)$ stretching vibrations originating from the 1,2,3-triazole group in compounds **1a–3a** are in the range of 1519–1520 cm^{-1}. Aliphatic C-H stretching peaks were observed in the range of 2850–2950 cm^{-1}. When the FTIR spectra of the 1,2,3-triazole oxime derivatives (**1b–3b**) are examined, the stretching vibrations of the aldehyde groups $\bar{\upsilon}(C=O)$ in the 1,2,3-triazole compounds have completely disappeared. Instead, $\bar{\upsilon}(C=N)$ stretching vibrations resulting from the imine bond in the oxime group in the FTIR spectra of the compounds were observed in the range of 1609–1610 cm^{-1}. The broad band observed in the 3150–3175 cm^{-1} region in the spectra of the 1,2,3-triazole oxime derivatives (**1b–3b**) is due to stretching vibrations belonging to the $\bar{\upsilon}(O\text{-}H)$ group. Aliphatic C-H vibrations in the compounds were observed as weak peaks in the range of 2900–3000 cm^{-1}. In addition, the peaks observed around 1510–1520 in the FTIR spectra of 1,2,3-triazole oxime derivatives originate from the 1,2,3-triazole group. The characteristic peaks in the FTIR spectra of 1,2,3-triazole (**1a–3a**) and 1,2,3-triazole oxime compounds (**1b–3b**) are in harmony with the spectra of similar compounds in the literature (Kose et al., 2017; Şahin, Bingöl, Onur, Güngör, Köse, Gülçin, Tümer, 2022).

^{1}H/^{13}C NMR spectra of the synthesized compounds were taken in CDCl$_3$. When the ^{1}H NMR spectra of 2-oxopropargyl-benzaldehyde compounds (**1–3**) were examined, the aldehyde group proton (CH=N) was observed as a singlet peak at 10.50 ppm. Singlet peaks in the range of 4.86–4.92 ppm in their spectra are due to OCH$_2$- protons. The proton (-C≡CH) belonging to the terminal alkyne group was observed at 2.61 (compound **1**), 2.49 (compound **2**) and 2.50 ppm (compound **3**). Methoxy group protons (-OCH$_3$) were observed at 3.91 ppm in compound 2, while protons belonging to the ethoxy group in compound 3 were observed as multiplet signals at 4.14 (-OCH$_2$CH$_3$) and 1.48 ppm (-OCH$_2$CH$_3$). The aromatic group protons in the compounds were observed in the range of 7.89–7.10 ppm. The integration values of the proton signals observed in the ^{1}H NMR spectra of the 2-oxo-propargylbenzaldehyde compounds (**1–3**) were found to be compatible with the proposed structures. When the 1H NMR spectra of the oxopropargylbenzaldehyde compounds (**1–3**) were examined, the carbon signals of the aldehyde group were observed at 189.57, 190.52 and 190.61 ppm, respectively. The carbon signals of the phenyl ring were observed in the range of 159.74–113.19 ppm. The terminal alkyne carbon atoms belonging to the propargyl group resonate in the range of 78–76 ppm. Signals of carbon atoms -OCH$_2$- found in the propargyl group of compounds were observed at 56.35 (comp. 1), 60.79 (comp. 2) and 64.56 (comp. 3) ppm. In compound 2, the methoxy group carbon signal was observed at 55.98 ppm, while in compound 3, the ethoxy group carbons were observed at 60.66 and 14.78 ppm. NMR spectra of compounds are in agreement with literature data (Şahin et al., 2021).

When the ^{1}H NMR spectra of the 1,2,3-triazole compounds (**1a–3a**) are examined, the peaks originating from the terminal alkyne protons, observed at about 2.50 ppm in the spectra of the starting compounds (**1–3**), disappear upon click reactions and the formation of the 1,2,3-triazole ring. In addition, in the ^{1}H NMR spectra of compounds **1a–3a**, the proton belonging to the 1,2,3-triazole group was observed as a single signal at 8.05 (compound **1a**) and 7.98 (compound **2a** and **3a**) ppm, respectively. In the spectra, hydrogen atoms belonging to the aldehyde group were observed as single peaks at 10.51 (compound **1**), 10.35 (compound **2**) and 10.50 (compound **3**) ppm. Single signals observed in the range of 5.43–5.46 ppm in the spectra originate from the protons belonging to the bridging OCH$_2$- group. The methoxy group proton signals in the compounds resonated in the range of 3.98–3.87 ppm. The multiplet peaks observed at 41.9 and 1.54 ppm in the spectrum of Compound **3a** are due to protons belonging to the ethoxy group. In compounds, aromatic proton signals were observed as multiplet signals in the range of 7.64–6.95 ppm. In the ^{13}C NMR spectra of 1,2,3-triazole-aldehyde compounds (**1a–3a**), the signal of the carbon atom (C=O) in the aldehyde group was observed at 189.62, 190.25 and 190.31 ppm, respectively. Carbon signals in the 1,2,3-triazole ring were observed at approximately 144 and 114 ppm. Other aromatic carbon atoms in the compounds resonated in the range of 160.43–112.81 ppm. The carbon atom signals of the -OCH$_2$- bridge in compounds (**1a–3a**) were observed at 62.48, 67.07 and 65.85 ppm, respectively. The methoxy group carbon atoms in the compounds were observed in the range of 55.63–56.12 ppm. The signals observed at 64.99 and 14.90 ppm in the spectrum of Compound **3a** originate from the ethoxy group carbon atoms. NMR data of 1,2,3-triazole-aldehyde compounds are compatible with similar compounds in the literature (Güngör et al., 2022).

When the ^{1}H NMR spectra of the synthesized 1,2,3-triazole oxime derivatives (**1b–3b**) were examined, it was observed that the carbonyl group proton (CH=O) signal disappeared in the output 1,2,3-triazole compounds (**1a–3a**). In addition, the peaks observed in the spectra of compounds **1b–3b** at 8.54, 8.44 and 8.45 ppm, respectively, are due to the imine bond protons. The aromatic C-H proton signal in the 1,2,3-triazole ring resonated at 8.00 (compounds **1b** and **2b**) and 7.99 (compound **3b**) ppm. In addition, the -OH group proton of the oxime group in the 1,2,3-triazole oxime derivatives was observed as a broad band around 8.25 ppm. Multiplet proton signals observed in the range of 7.65–6.96 ppm in the spectra originate from aromatic hydrogen atoms. The hydrogens in the -OCH$_2$- bridge group in the compounds gave a peak in the range of 5.30–5.40 ppm. The methoxy group protons in the compounds were observed as singlet peaks in the range of 3.80–3.90 ppm. Hydrogens belonging to the ethoxy group in the structure of compound **3b** were observed as multiplet signals at 4.17 and 1.51 ppm. In the

^{13}C NMR spectra of the compounds (**1b–3b**), the carbon peaks of the imine bond were observed at 159.97, 159.86 and 159.85 ppm, respectively. Carbon atoms in the 1,2,3-triazole ring were observed at about 144 and 114 ppm. Other aromatic carbon atoms in the compounds were observed in the range of 156.19–112.63 ppm. The carbon atoms of the bridging OCH$_2$- group resonated in the range of about 62–65 ppm. The carbon atoms to the methoxy groups peaked at approximately 55–56 ppm. In compound **3b,** ethoxy group carbons were observed at 64.32 and 14.94 ppm.

3.2. Crystal structures of compounds 3, 2b and 3b

Single crystals of compounds **3**, **2b** and **3b** were obtained by recrystallization from the ethyl acetate solution of the compounds. The crystal structures of the compounds were determined by single-crystal X-ray diffraction studies. According to X-ray diffraction data, compounds **3**, **2b** and **3b** were found to crystallize in the triclinic unit cell and P-1 space group. The crystal structure of compound **3** is shown in Figure 2(a). The asymmetric unit contains one molecule. The C7-O1 bond length of the aldehyde group in the compound was found to be 1.198(5) Å, and this distance is the characteristic C=O double bond length. The C9-C10 bond length of the terminal alkyne group in the compound is 1.157(4) Å and has C≡C triple bond character. Two molecules in the crystal structure formed a dimer structure by supramolecular interaction with the aldehyde group and the terminal alkyne hydrogen [C9≡C10-H⋯O1, the donor-acceptor (C10⋯ O1) distance is 3.129(5) Å (Figure 2(b)). The molecules in the crystal structure formed a one-dimensional lattice with CH⋯O interactions (Figure 2(c)).

The crystal structure of 1,2,3-triazole oxime compound (**2b**) is shown in Figure 3. While there are 12 molecules in the unit cell, there are 6 molecules in the asymmetric unit. The bond angles and lengths of the molecules in the symmetric unit are similar, but the angles between the rings differ. The imine bond length (N7-N1) of the oxime group in the compound is 1.278(4) Å and it has C=N double bond character. The bond lengths of N2-N3, N3-N4, N4-C11, C11-C10 and C10-N2 in the 1,2,3-triazole ring are 1.311(4), 1.349(4, 1.333(5), 1.357(5) and 1.348(5) Å, respectively, and the obtained bond lengths show π-electron conjugation in the 1,2,3-triazole ring. The oxime group in the compound formed a hydrogen bond dimer by mutual intermolecular hydrogen bonds with one of the 1,2,3-triazole nitrogen atoms in the neighbouring molecule (Figure 4). The π interactions increased the stability of the crystal structure. The package diagram of the molecule is shown in Figure 5.

The crystal structure of compound **3b** is given in Figure 6. All bond lengths in the compound were found to be within the expected values. The C7-N1 bond length in the compound is 1.280(3) Å and this bond has C=N double bond character. The bond lengths in the 1,2,3-triazole ring in the compound range from 1.313 to 1.360 Å, indicating π-electron conjugation across the ring. The oxime group of a crystalline molecule and the 1,2,3-triazole group of the neighbouring molecule formed a dimeric structure by interacting with the intermolecular hydrogen bond [O1-H⋯ N2, donor(O1)-acceptor(N2) distance: 2.783(3) Å]. (Figure 7(a)). In the crystal
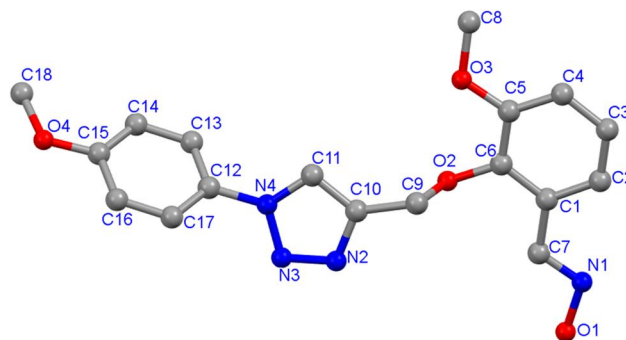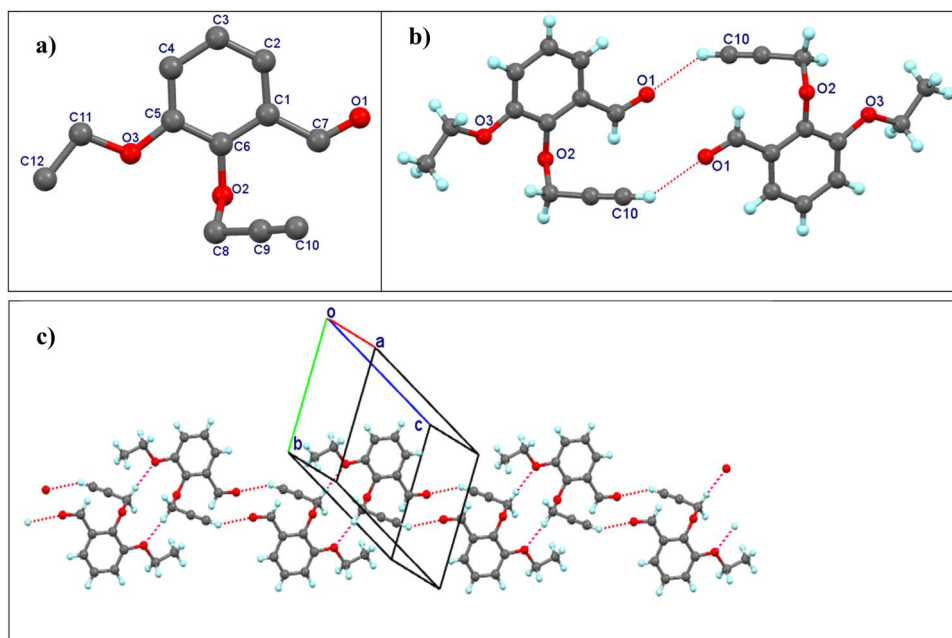

Figure 3. Crystal structure of compound **2b** with numbered atoms.

Figure 2. (a) Crystal structure of compound 3. (b) Dimer formation by C≡C-H⋯O interactions. (c) Packing diagram showing CH⋯O interactions in one dimension.

structure, the 4-methoxybenzene ring directly attached to the 1,2,3-triazole group entered into π-π interaction with the same group in the neighbouring molecule (Figure 7(b)). Molecules formed a two-dimensional supramolecular structure *via* π-π stacking interactions. The packing diagram of the molecule is given in Figure 8.

3.3. DNA binding studies

3.3.1. Absorption spectroscopic studies

Since DNA is the carrier of genetic information, examining DNA-small molecule (potential drug candidate molecules) interactions is important for the development of new drug candidate molecules in the field of pharmacology, tumorigenesis or pathogenesis. DNA can interact with drug-candidate molecules in different ways. One of the electronic spectroscopy methods, UV–vis absorption titration, is among the most effective methods used to find the DNA binding mode. In general, when drug molecules interact with DNA to form a new complex, absorbance values are reduced (hypochromism) or increased (hyperchromism) and/or a bathochromic (red shift) or hypsochromic (blue shift) effect is produced (Feizi-Dehnayebi et al., 2022). In general, a decrease in absorption intensity and redshift is caused by strong interactions, such as intercalation. On the other hand, weak interactions, such as electrostatic or groove bonding, do not lead to a shift (Aleksić

& Kapetanović, 2014). When the DNA molecule interacts with the compound, the π orbitals of the DNA base pair and the compound can combine, resulting in a bathochromic effect. The resulting bathochromic effect indicates the intercalation binding mode. Denaturation and damage to the DNA double helix result in hyperchromic changes. In the case of strong
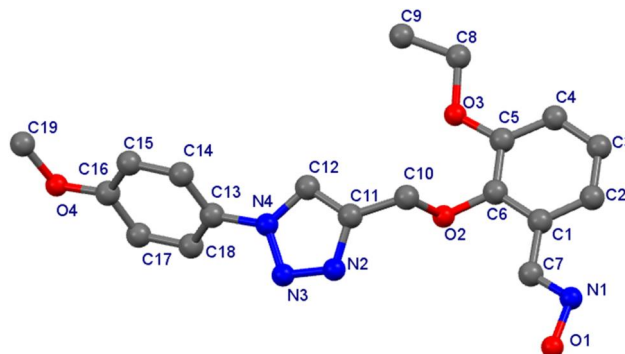

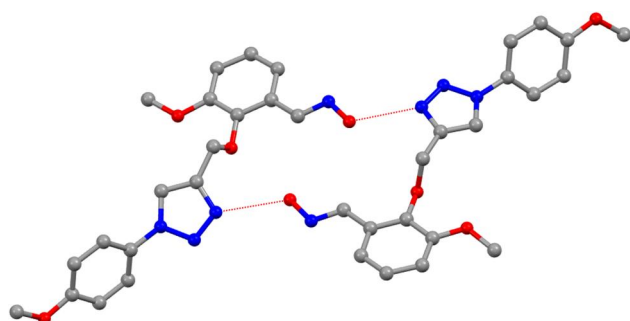**Figure 6.** Crystal structure of compound **3b** with numbered atoms.

Figure 7. Hydrogen bond dimer formation (a) and π–π stacking interaction (b) in compound **3b**.

Figure 4. Hydrogen bond dimer in the crystal structure of compound **2b**.
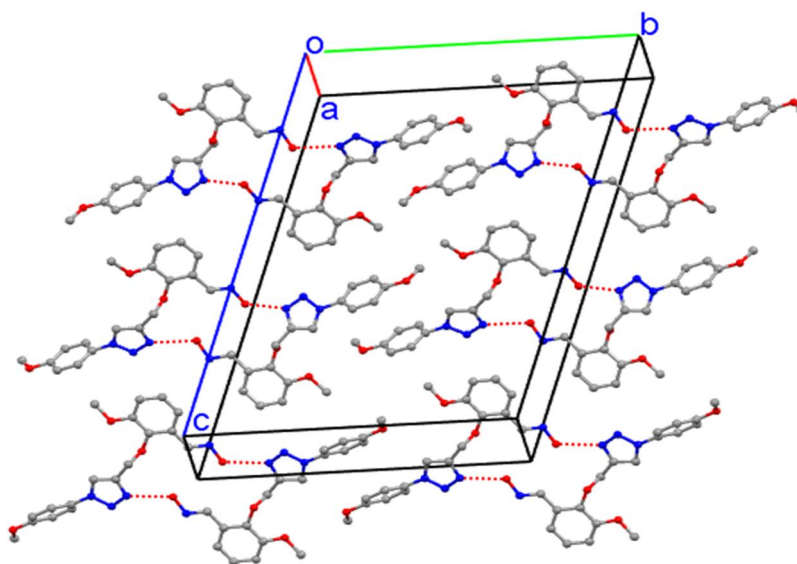

Figure 5. Packing diagram of compound **2b**.

interactions with DNA, no shift is seen, whereas in the case of weaker interactions (trough binding and electrostatic interactions) no shift is seen (Aleksić & Kapetanović, 2014).

vBy fixing the concentration of 1,2,3-triazole compounds and their oxime derivatives with increasing DNA concentration, the absorption spectra were recorded in Figures 9 and 10. The K_b constants of the compounds are given in Table 1. When the absorption spectra of compounds **1a–3a** were examined, two bands were observed around 240 and 324 nm,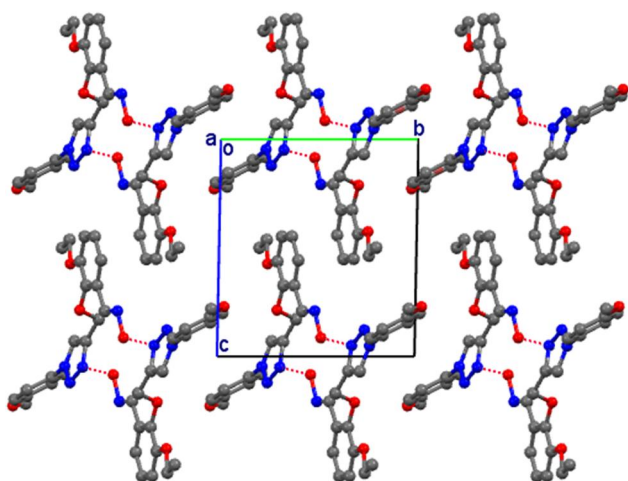 respectively. The high energy band around 240 nm is due to the π-π* transition. As DNA concentration increased, hyperchromism (∼40%) and bathochromic effect (∼5%) were observed in the first band. Hypsochromic (∼15%) and bathochromic (∼5%) effects were observed in the second peak. It was observed that the changes observed in the UV–vis absorption bands of the compounds, included hypsochromic and bathochromic effects together with hyperchromism. These results directly showed that the interaction of the compound with FSdsDNA. In general, in the case of intercalation, the π-bonded orbital of the intercalated molecule can couple with the π-bonded orbital (π) of the DNA base pairs, resulting in the decrease of the π-π* transition energy and the bathochromic (red shift) (>10 nm) of the absorption band. In addition, the electronic transition probability decreases and hypochromism appears (up to 40%) due to the partial filling of the coupling π orbital by electrons. This hyperchromicity reflects changes to DNA structure and conformation that occur when DNA interacts with small molecules. This is due to the fact that the electronic states of the chromophore of the complex overlap with the nitrogen bases in the grooves of the DNA. From the foregoing, it can be concluded that there is a binding interaction between DNA and gefitinib and that the main binding mode may be the groove binding interaction. The spectrophotometric results obtained suggest that the compounds interact with DNA *via* non-intercalative binding mode.

The change in the structure of 1,2,3-triazole derivatives with the addition of the oxime group to the structure caused a spectral effect with a significant difference. Compounds **1b**,
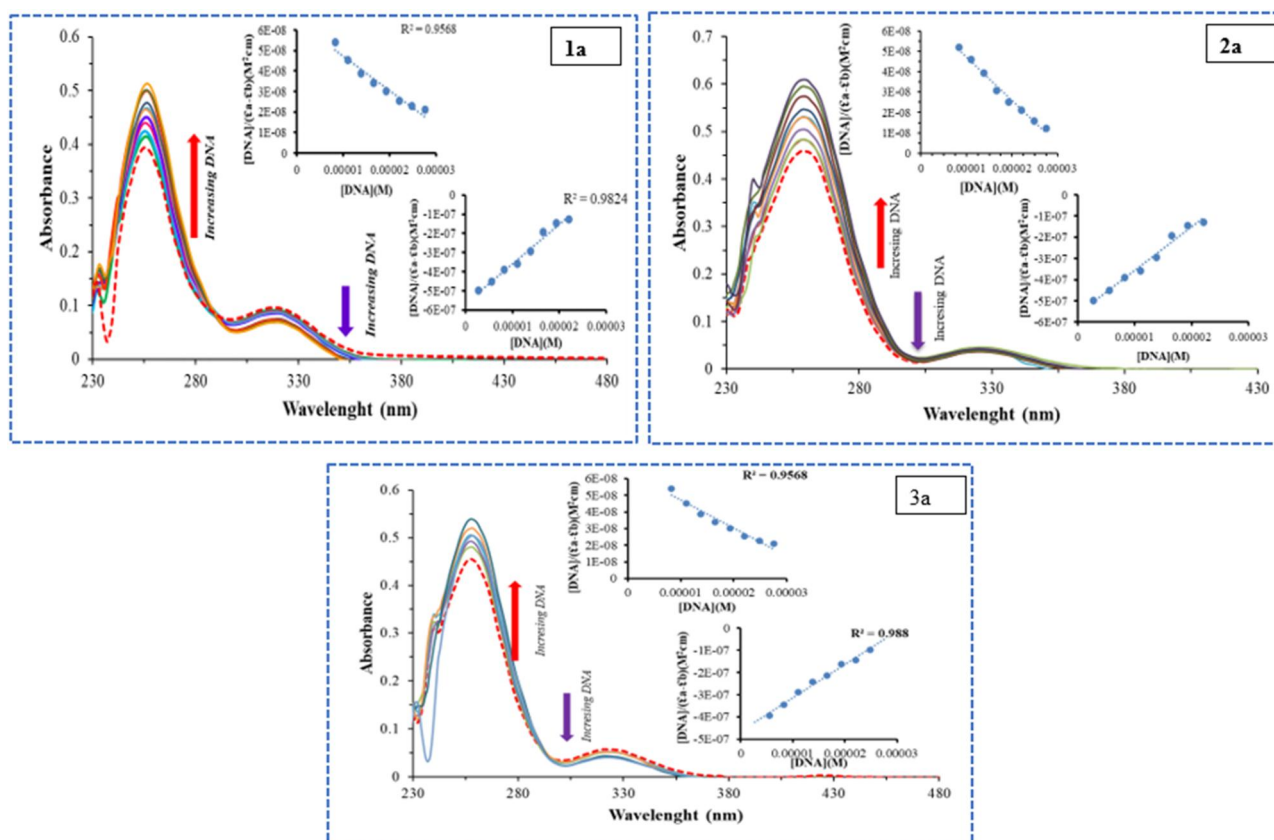

Figure 8. Packing diagram of compound **3b**.

Figure 9. Absorption spectral changes of compounds, in 2 mM Tris–HCl/2 mM NaCl buffer at pH 7.1 upon the addition of FSsdDNA. Insets: [DNA]/□a–□f) *versus* [DNA] plot for the titration of FSsdDNA with compounds, experimental data points; full lines, linear fitting of the data. [compound] 2.50×10^{-5} M, [DNA] 0–1000 μM.
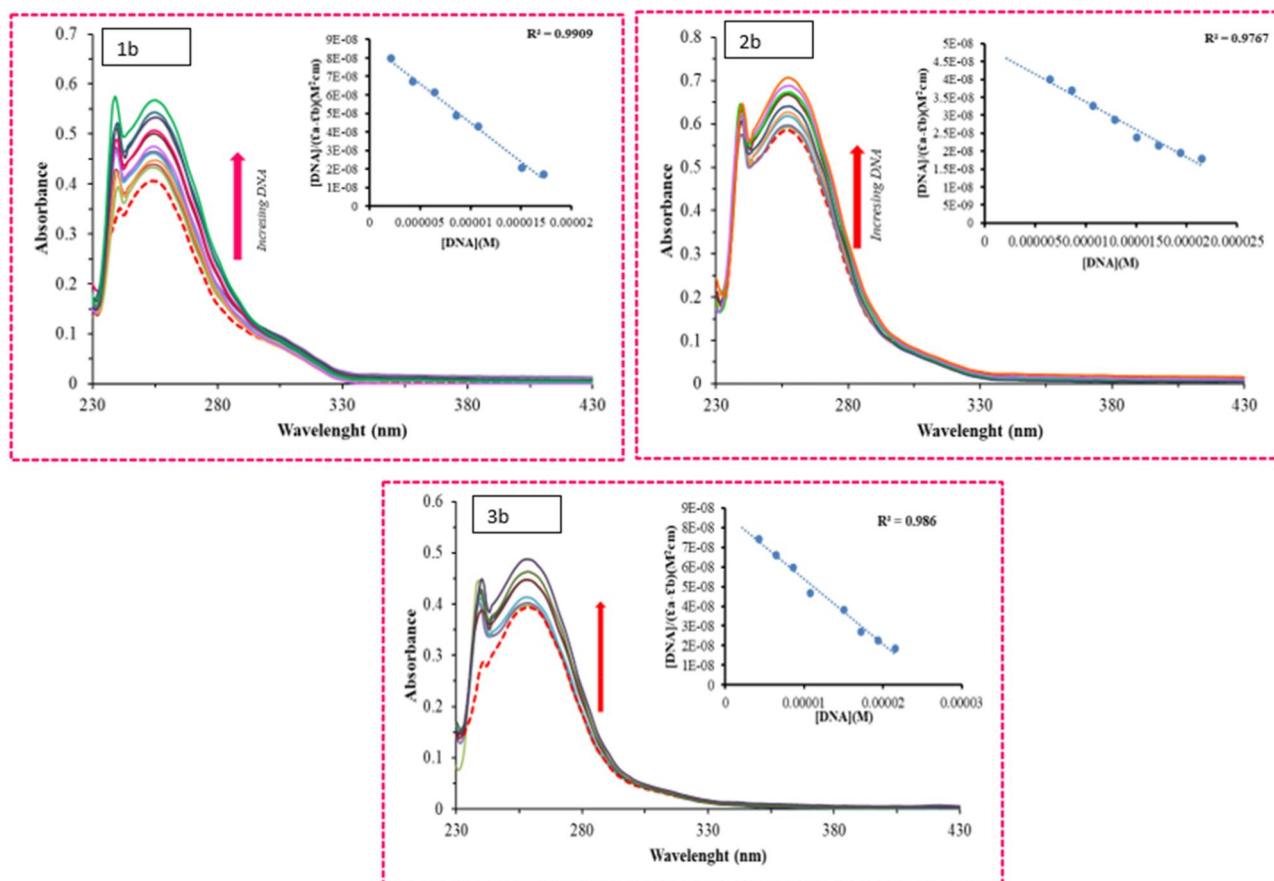
Figure 10. Absorption spectral changes of compounds, in 2 mM Tris–HCl/2 mM NaCl buffer at pH 7.1 upon the addition of FSsdDNA. Insets: DNA]/(εa−εf) *versus* [DNA] plot for the titration of FSdsDNA with compounds, experimental data points; full lines, linear fitting of the data. [compound] 2.00×10^{-5} M, [DNA] 0–1000μM.

Table 1. The values of the DNA binding and EB-displacement binding constants of the compounds.

Compound	[a]K_{b1} 10^4 (M^{-1})	[a]K_{b2} 10^4 (M^{-1})	[b]K_{sv} 10^4 (M^{-1})	[c]K_f 10^{11} (M^{-1}S^{-1})	[d]n	logK_b	[e]K_{app} 10^4 (M^{-1}S^{-1})
1a	3.45	28.0	1.08	1.08	1,35	5.40	6.83
2a	3.88	31.0	1.04	1.04	1,30	5.23	1
3a	3.95	34.2	1.04	1.04	1.08	4.31	9.37
1b	33.6	–	1.13	1.13	1.19	4.85	0.75
2b	30.5	–	1.08	1.08	1.13	4.59	6.81
3b	46.6	–	1.14	1.14	1.204	4.85	8.33

a: binding constants b: Stern–Volmer constant c: quenching constants d: number of binding sites e: apparent binding constant.

2b and **3b** exhibited two maximum absorptions at 240 and 260 nm (Figure 10). As described for all bioligands studied, the two bands showed mixed changes with bathochromic shifts of gradually increasing intensity (hyperchromism) upon addition of small amounts of deoxyribonucleic acid. When FSdsDNA is subsequently added, hyperchromism with a slight red shift is observed between **1b–3b**. This is indicative of complex formation. Slotted binding appears to be a more acceptable mode of binding in combination with the slight red shift and hyperchromatic electrostatic interaction observed in the peak. Formation of **1b–3b** DNA complexes is demonstrated by this experiment. It also provided an initial idea that the binding mode was groove binding. The UV–vis spectral data were used to determine the value of the binding constant (K_b), which describes the strength of the interaction between the compounds and the DNA.

The K_b values of the compounds range from 3.05×10^4 to 4.66×10^5 M^{-1} when the binding constants given in Table 1

are evaluated. The binding constants of 1,2,3-triazole and their oxime derivatives are **3b> 1b> 2b > 3a > 2a >1a**. Examination of the data in Table 1 shows that compound **3b** binds much more strongly to DNA than the others. The classical minor groove binding mode was determined from the binding constant (K_b) values of the compounds. They were also found to be higher than those of spermine (K_b = 3.38 $\times 10^5$ M^{-1}). It was clear that the compounds were bound by FSdsDNA *via* groove binding based on the magnitude of these binding constant values. This could be due to the hydrophobicity of ethyl moiety in compound **3b.** This increases the binding strength to the DNA base pair.

3.3.2. Competitive binding studies
Fluorescence quenching experiments were performed using a DNA dye and cationic ethidium bromide with a specific binding mode with DNA to detect DNA interaction. In this
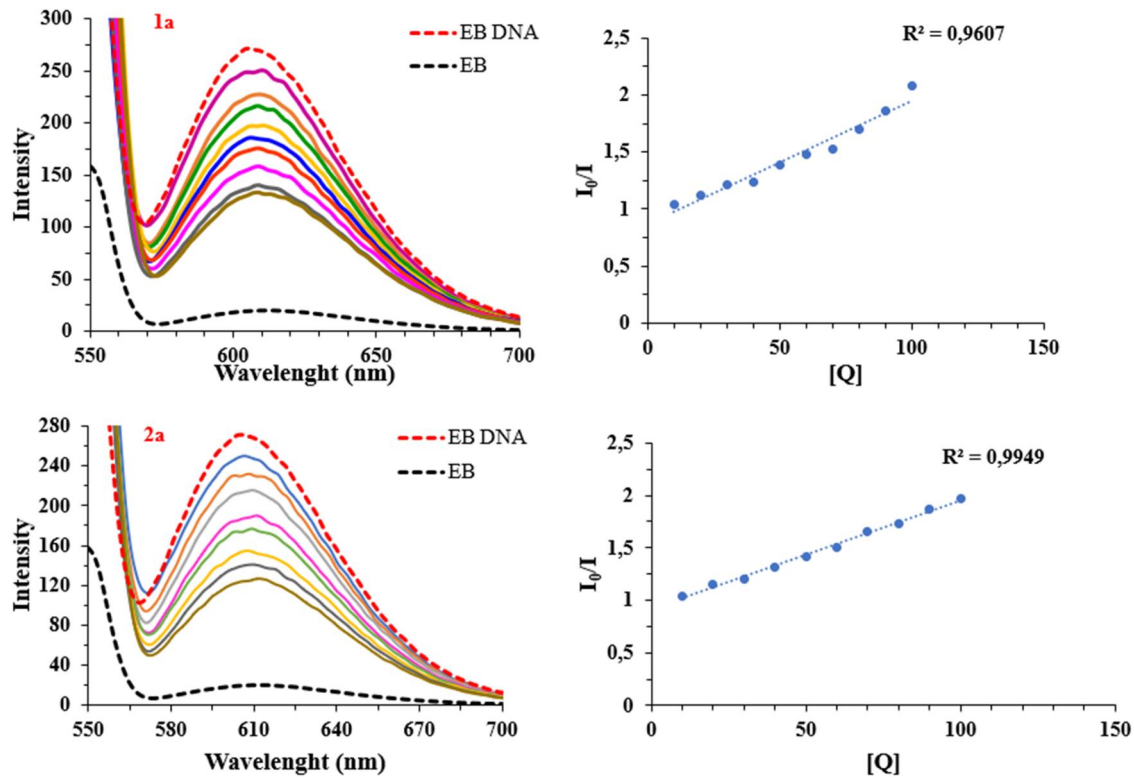
Figure 11. Effect of addition of compounds **1a–2a** the emission intensity of the EB-FSdsDNA complex (75 µM) at different concentrations (0–110 µM) in 2 mM Tris–HCl buffer (pH = 7.1) and Stern–Volmer plot of fluorescence titrations of the compounds with EB-FSdsDNA.
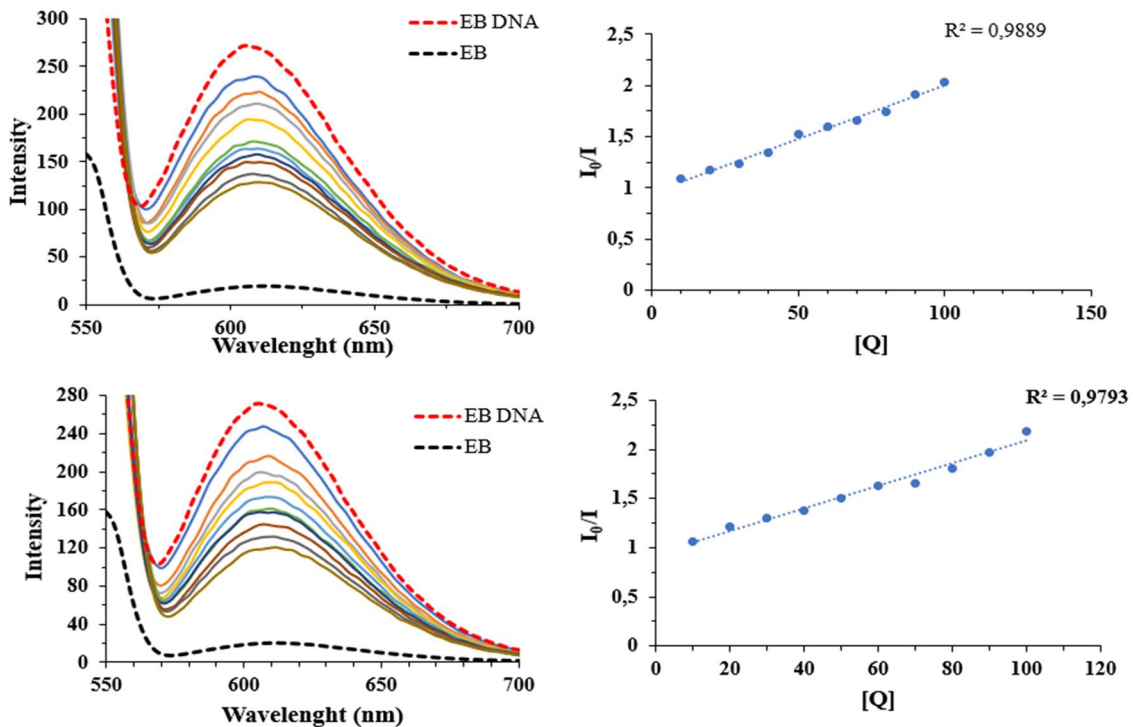

Figure 12. Effect of addition of compounds **1b–2b** the emission intensity of the EB-FSdsDNA complex (85 µM) at different concentrations (0–100 µM) in 2 mM Tris–HCl buffer (pH 7.1) and Stern–Volmer plot of fluorescence titrations of the compounds with EB-FSdsDNA.

study, the emission band was observed at 526 and 610 nm. Fluorescence quenching was observed with the gradual addition of compounds at various concentrations to EB-FSdsDNA. This caused EB to be replaced by compounds or by binding to different base pairs of DNA causing quenching (Links et al., 2012). Spectra of **1a–2a** and **1b–2b** compounds are shown in Figures 11 and 12. The K_{sv} of the compounds are given in Table 2. It was observed that the compounds at the tested concentration did not cause dramatic fluorescence quench, suggesting the no replacing of EB from DNA-EB

Table 2. Interaction of compounds with BSA.

Compound	Temperature (K)	[a]$K_{sv} \times 10^4$ (M^{-1})	[b]K_q 10^{11} (M^{-1}S^{-1})	[c]ΔG (Kj mol^{-1})	[d]ΔH (Kj mol^{-1})	[e]ΔS (J mol^{-1} K^{-1})
1a	298	5.6	5.6	−89,16	−24.75	−185.7
	300	5.04	5.04	−91.42		
	310	3.08	3.08	−64.45		
2a	298	7.54	7.54	−75.205	−59.27	−291
	300	6.77	6.77	−93.48		
	310	5.11	5.11	−105.46		
3a	298	8.19	8.19	−71.56	−47.17	−71.48
	300	6.95	6.95	−72.91		
	310	6.59	6.59	−75.56		
1b	298	8.19	8.19	−79.23	−95.66	−119
	300	7.05	7.05	−83.45		
	310	7.01	7.01	−86.78		
2b	298	5.79	5.79	−96.88	−41.85	−24.57
	300	5.43	5.43	−105.06		
	310	2.52	2.52	−112.44		
3b	298	6.9	6.9	−93.72	−50.23	−269
	300	4.6	4.6	−100.46		
	310	4.4	4.4	−111.49		

a: Stern–Volmer constant b: quenching constants c: Gibbs free energy change d: Enthalpy change e: Entropy change.
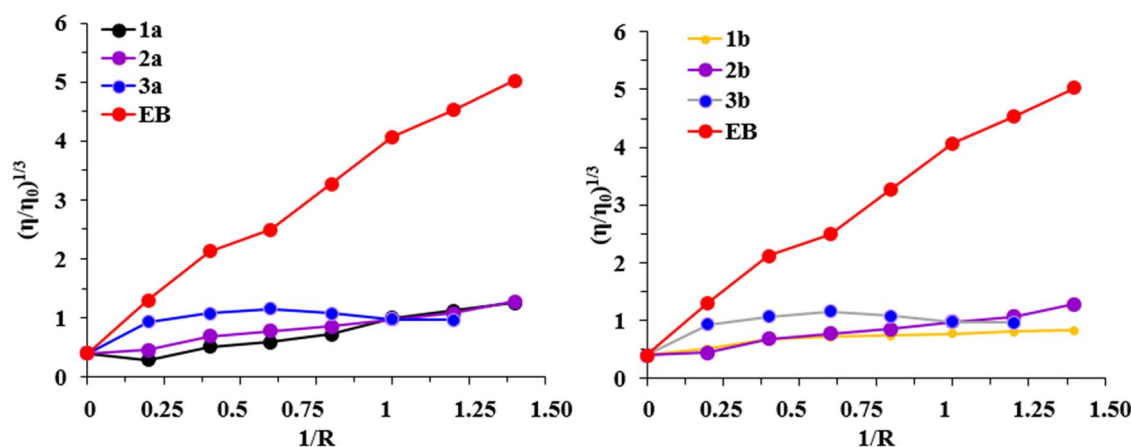
Figure 13. Relative viscosity experiment of 1,2,3-triazole and their oxime derivatives with FSdsDNA.

system (Güngör et al., 2021). Also, a slight redshift was observed when increasing amounts of compounds were added. Changes in K_{sv} (binding constant, M^{-1}) and n (binding site number) indicate a minor groove binding mode, which is consistent with non-competitive inhibition. The K_{app} values of all compounds (Table 2) are even lower than the K_{app} value of EB itself (10^7 M^{-1}) and do not reach the 10^5 M^{-1} discussed in the literature. There was also evidence that the compounds did not have any intercalation effects on DNA (Galindo-murillo et al., 2015).

3.3.3. Viscosity assay

The type of ligand that binds to DNA is determined by spectroscopic studies. However, the binding pattern of the ligand that binds to DNA cannot be determined from these studies alone. Therefore, relative viscosity experiments were performed to fully understand the compounds-DNA interaction. As the compound enters between the two parts of the DNA molecule, it causes an increase in the viscosity of the DNA solutions (Street, 1995). In the case of groove binders (Elghiaty et al., 2023), molecules that bind to the DNA surface, a very small change in viscosity is observed. It is known that

a decrease in relative viscosity is observed with the covalent binding of compounds to DNA (Butour & Macquet, 1981).

By adding a compound to DNA, it can cause elongation, shortening or dissolution of the helix in the DNA structure. EB is known to complex with DNA. That EB intercalates between the DNA chain in this complex is also known from the literature. When we carried out the viscosity study, the slope in the case of EB was almost 10 times higher than those of the compounds, confirming that the compounds were placed in the grooves of DNA and were not intercalated (Figure 13).

3.4. BSA binding studies

To study the quenching mechanism of BSA with compounds, fluorescence spectroscopy is the most effective method (Ray et al., 2012). When excited at 295 nm, BSA has a strong fluorescence emission at 344 nm, as mentioned above (Toneatto & Argüello, 2011). The excitation of the tyrosine and tryptophan residues in the protein is responsible for the 280 nm excitation wavelength. Spectra of BSA at three different temperatures (290, 303 and 310 K) in presence and absence of various compounds are shown in Figure 14. The intensity of the fluorescence diminishes as the concentration of the
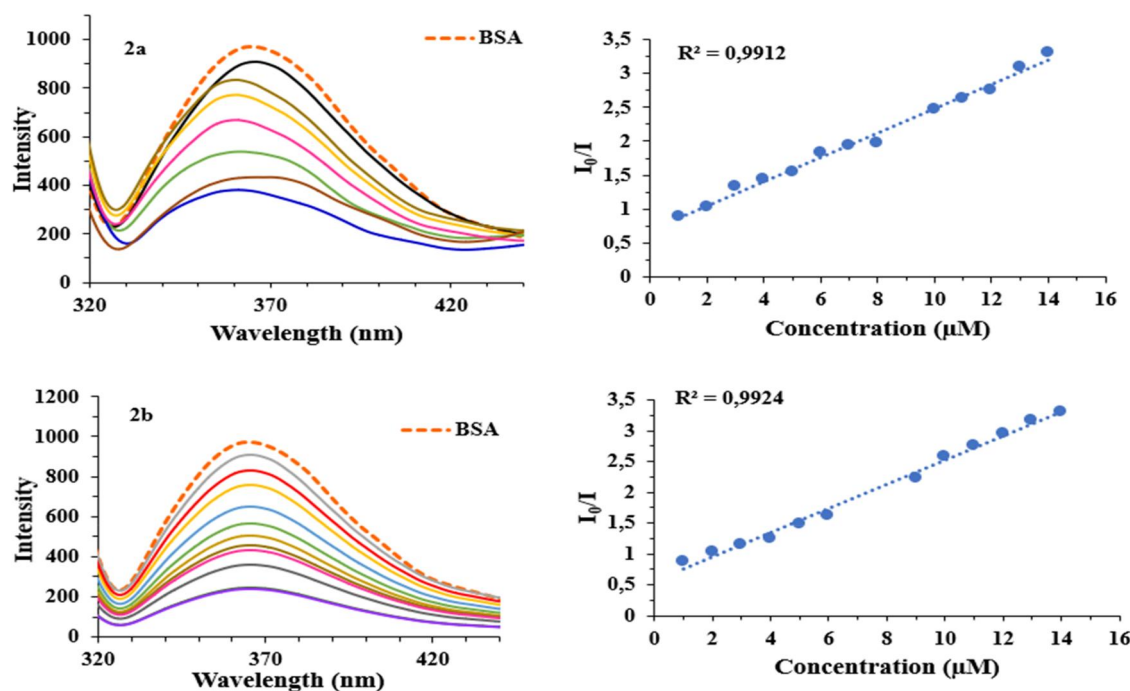
Figure 14. Fluorescence emission spectra of BSA (2 μM) in the absence and presence (10–100 μM, respectively) of compounds **2a–2b** (λ_{exc} = 295 nm).

substance increases, but the maximum emission wavelength does not change. The data show that the compound quenches fluorescence. K_{sv} (dynamic quenching constant) and K_q (quenching rate constant of BSA) were calculated using the equation to explain the quenching mechanism of the compound (Chowdhury et al., 2006). K_{sv} values were calculated from the slope of the I_0/I and [Q] graph at different temperatures. If the K_{sv} value increases with increasing temperature, it has a dynamic quenching mechanism, if it decreases as the temperature increases, it has a static quenching mechanism. Table 2 shows the calculated K_{sv} and K_q values for the interaction of the compounds with BSA at different temperatures. The calculated K_{sv} values have an inverse relationship with temperature, supporting the mechanism of static quenching, as shown in Table 2. Among the synthesized compounds, the oxime derivatives **1b** and **3b** had larger K_{sv} values. The hydrogen bonding with the proteins in the structure of BSA may be responsible for the -OH groups formed in the structure. The maximum K_q value of the different extinguishing agents with biological macromolecules is 10^{10} M^{-1} s^{-1} (Ware, 1962). In this study, the K_q values of the quenching processes (10^{13} M^1 s^1) are greater than 10^{10} M^1 s^1. These results confirm that quenching is not initiated by a dynamic mechanism. Instead, it is due to the formation of a compound resulting from the static quenching mechanism (Zhang et al., 2007).

Thermodynamic parameters (ΔH and ΔS) were calculated to predict the nature of the interactions. (i) $\Delta H < 0$ and $\Delta S < 0$ are hydrogen bonds and van der Waals forces; (ii) $\Delta H > 0$ and $\Delta S > 0$ are hydrophobic forces; and (iii) $\Delta H > 0$ and $\Delta S < 0$ are electrostatic (Feizi-dehnayebi et al., 2021).

The values for ΔH and ΔS were obtained by plotting the $1/T$ absolute temperature *versus* the $\ln K_b$ curve in accordance with the van't Hoff equation. Table 2 shows the thermodynamic parameters obtained for BSA binding. On the basis of the information presented in Table 2, van der Waals and hydrogen bonding are the most important interactions in the binding of BSA, as both ΔH and ΔS are negative. Changes in the Gibbs free energy (ΔG) have also been determined. The values of ΔG for the BSA binding are negative. This indicates spontaneous processes.

3.5. AChE/BChE enzyme inhibitory activities

Alzheimer's is caused by a decrease in an individual's ability to synthesize ACh, leading to progressive neurodegeneration (Francis et al., 1999). The cognitive deficits observed in Alzheimer's patients with low ACh receptor binding led researchers to hypothesize that increasing the availability of ACh in the brain may reduce Alzheimer's-related cognitive decline. At the same time, BChE may be considered a clinical target in the AD process, as it may take over the function of AChE in regulating cholinergic signalling. ChEIs inhibit AChE and BChE activity (reversibly or irreversibly), increasing ACh and BChE levels. FDA-approved cholinergic drugs on the market include rivastigmine, donepezil and galantamine (GNT), which increase ACh levels by inhibiting AChE activity. However, most of these drugs have been shown to have side effects such as gastrointestinal upset and liver toxicity. The inhibitory activities of **1a–3b** compounds against AChE (from electric eel) and BuChE (from horse serum) have been evaluated using the Ellman method. The reference compounds used were GNT and rivastigmine. The results are summarized in Table 3. It was determined that all synthesized compounds had IC_{50} values ranging from 46.73 to 4.8 μM for AChE and 100.01–70.16 μM for BuChE. It was determined that the synthesized 1,2,3-triazole and their oxime derivatives were more active against AChE enzyme. Among the synthesized compounds, **1b**, **2b** and **3b**

Table 3. The IC_{50} values of the compounds AChE and BChE.

Compound	AChE inhibition [IC_{50} (µM)]	BChE inhibition [IC_{50} (µM)]	Selectivity for AChE[a]
1a	46.73 ± 0.03	82.01 ± 0.11	1.75
2a	34.46 ± 0.21	95.21 ± 0.06	2.76
3a	63.92 ± 0.14	83.68 ± 0.08	1.30
1b	10.67 ± 0.14	100.01 ± 0.19	9.37
2b	8.6 ± 0.05	79.02 ± 0.09	9.18
3b	4.8 ± 0.052	70.16 ± 0.89	14.61
Galantamine	13.56 ± 0.01	16.32 ± 0.2	–

[a]IC_{50} (BuChE)/IC_{50} (AChE).
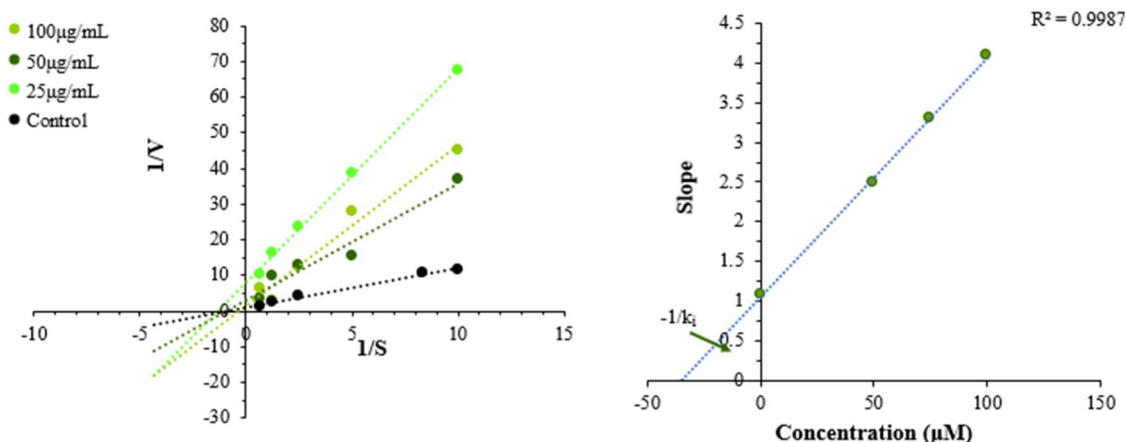
Figure 15. Compound **2b** kinetic study of BuChE inhibition. BuChE initial velocity with increasing substrate concentration is shown. To construct the secondary plot shown in panel, the slopes of the lines for 1/V *versus* 1/[S] from the LWB plot were plotted against inhibitor concentration. V = initial velocity rate, [S] = substrate concentration, [I] = inhibitor concentration **2b**.

compounds with oxime structure were found to have higher ACh enzyme inhibition activity. It is thought that the -OH groups in the structure provide inhibition of the enzyme through hydrophobic or hydrophilic interactions. Among 1,2,3-triazole oxime derivatives, it was observed that compound **3b** had a higher activity against ACHE (IC_{50} = 4.8 mM) and BuChE (IC_{50} = 70.16 mM). It was found that the ethyl group in the structure was effective in enzyme inhibition. It is thought that the ethyl group plays a role in inhibiting the enzyme by making Van der Waals interactions with the residues of the protein in the cas part of the enzyme. Compounds **2b** and **3b**, which are oxime in their structure, were found to be approximately twice as active for AChE when compared to the standard component GNT. In our opinion, compounds **2b** and **3b** were found to show increased inhibitory activity against AChE and 6.2- and 6.6-fold higher selectivity for AChE over BuChE, respectively, compared with the positive control GNT.

3.6. Kinetic assay

A kinetic study was performed to determine the mode of inhibition of compounds **2b** and **3b** against AChE. Lineweaver–Burk binary *versus* graphs were generated using Ellman's procedure. Using different concentrations of substrate [S] in the presence and absence of inhibitor, the relative rate (v) of the enzyme was measured. After addition of the substrate, their respective curves were viewed at 412 nm for only 10 min. Then, to determine the type of inhibition, 1/Vmax *versus* 1/[S] was plotted using the slopes associated

with the curves. The slopes of this reciprocal plot were plotted against the concentration of the inhibitor to obtain the inhibitor constant. The Ki values for **2b** and **3b** were 3.50 ± 0.21 and 2.10 ± 0.35 µM, respectively, from a secondary plot of the slopes of the Lineweaver–Burk plots *versus* inhibitor concentration (Figures 15 and 16). These results suggest that **2b** and **3b** are potent non-competitive inhibitors of AChE. It also shows that it has a complex inhibition mechanism.

3.7. Molecular docking study

1,2,3-Triazoles and their oxime derivatives (**1a–3b**) were performed using AutoDock 4.2 software molecular docking studies to determine the ligand-protein interaction. AChE, BChE, BSA and DNA co-crystallized ligands GNT, tacrine (THA), (2S)-2-(6-methoxynaphthalen-2-yl)propanoic acid (NPS), and 2'-(4-hydroxyphenyl)-5-(4-methyl-1-piperazinyl)-2,5'-bi-benzimidazole (HT) were removed, respectively, and the mode of binding between protein and ligand was evaluated by performing the redocking procedure. Redocking procedure the co-crystallized ligands and relocated ligands redocking closely by overlapping with each other in the same position showed in Figure 17. The reliability of the redocking technique tested and approved that it docking with high accuracy. Docking was considered acceptable if the mean of the root mean square deviations (RMSDs) of the docking poses was less than the 2.0 Å threshold. In addition, GNT, THA, NPS and HT ligands relocated to the active site of the proteins and their co-crystallized ligands RMSD values were calculated
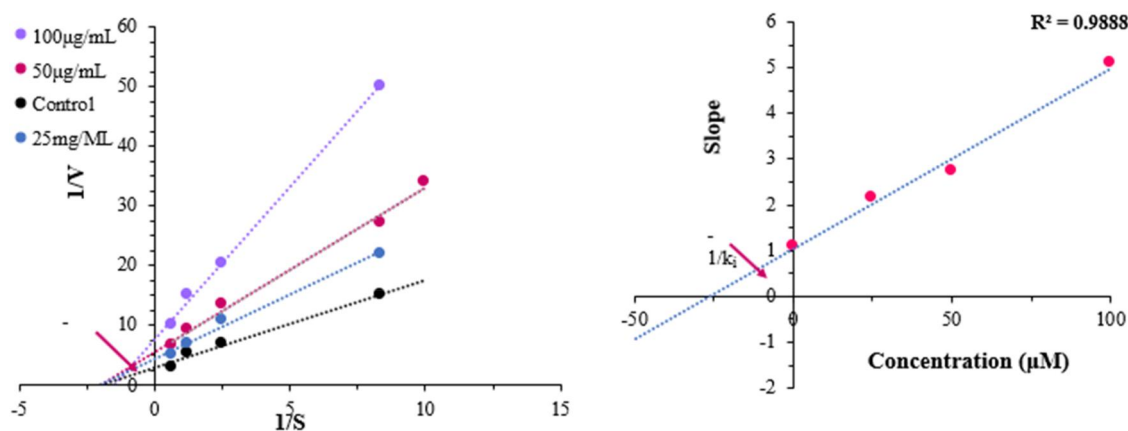
Figure 16. Compound **3b** kinetic study of BuChE inhibition. BuChE initial velocity with increasing substrate concentration is shown. To construct the secondary plot shown in panel, the slopes of the lines for 1/V *versus* 1/[S] from the LWB plot were plotted against inhibitor concentration. V = initial velocity rate, [S] = substrate concentration, [I] = inhibitor concentration **3b**.
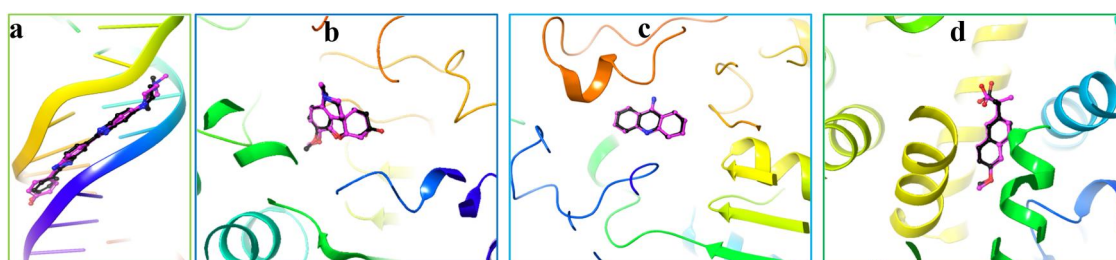

Figure 17. Docking validation. Receptors were depicted in the ribbon model which AChE (a) BChE (b), BSA (c) and DNA (d) The poses of co-crystallized ligands were represented in pink color ball and stick modelling while that of docked ligands is represented in black color ball and stick modelling.

Table 4. Binding affinities of **1a–3b** against AChE, BChE, BSA and DNA.

Compounds	Binding affinities (kcal/mol)			
	AChE	BChE	BSA	DNA
1a	−9.42	−9.26	−9.28	−9.58
2a	−9.67	−8.97	−9.51	−983
3a	−9.41	−9.46	−9.64	−9.83
1b	−9.82	−8.93	−9.68	−9.76
2b	−9.95	−9.77	−9.31	−9.81
3b	−10.17	−9.79	−9.47	−10.03
GNT	−9.37	–	–	–
THA	–	−7.77	–	–
NPS	–	–	−8.29	–
HT	–	–	–	−13.16

GNT: galantamine; THA: tacrine; NPS: (2S)-2-(6-methoxynaphthalen-2-yl)propanoic acid; HT: 2′-(4-hydroxyphenyl)-5-(4-methyl-1-piperazinyl)-2,5′-bibenzimidazole

as 0.692, 0.142, 1.414 and 0.518 Å, respectively. All compounds were inserted into the active site of the proteins by applying the redocking procedure to detect their possible binding poses, interactions and affinities towards AChE, BChE, BSA and DNA. The affinities of all compounds and their best poses are given in Table 4.

Molecular insertion results show that all compounds prefer to insert into the minor groove of the DNA double helix with binding energies ranging from (−9.58 kcal/mol) to (−10.03 kcal/mol). Docking results of the compounds are given in Table 4. According to this insertion result, the binding affinity of the DNA double helix natural reference HT compound is −13.16 kcal/mol. Compared to reference compound HT, 3b exhibited the best inhibitory property, with the lowest binding affinity −10.03 kcal/mol among the compounds. **3b** binding modes and interaction types are given

in Figure 18. The oxime group of **3b** was interacted by hydrogen bonding with the phosphate group (−1.9, 2.7 and 3.0 Å) on DT8 located in the DNA double helix. Also, **3b** made hydrogen bond (2.3 Å) between the DA6 nucleotide. **3b** were contribute to the stable conformation by making non-covalent and hydrophobic interactions between DNA double helix. Docking results revealed the presence of significant interactions between **3b** and DNA inserted into the minor groove of DNA. The binding modes of other compounds are given in Figure S19 in Supplementary file.

Docking study was performed to investigate further details behind the quenching activity of compounds on fluorescence with BSA. The binding energies of the compounds ranging from (−9.28 kcal/mol) to (−9.68 kcal/mol) as a result of placement were presented in Table 4. According to these docking results, **1b** (−9.68 kcal/mol) showed stronger inhibitory activity than reference NPS (−8.29 kcal/mol) and other compounds. As a result of docking, the binding modes and interactions of the most stable conformation of the binding energy in the subdomain IIA active region (Giannousi et al., 2020) of the most active compound **1b** were given in Figure 19. Compound **1b** shows various interactions with important amino acids in subdomain IIA of BSA. Compound **1b** makes hydrogen bonding with Lys350 (1.9 and 2.0 Å), Leu480 (2.1 Å) and Val481 (2.6 Å) amino acids. The ring containing the methoxy group made pi-pi interaction with Tyr213 (3.83 and 5.46 Å) amino acid. The results from the experimental and molecular docking analysis confirm each other. The reductions in the titration graph at 295 nm in **1b** -BSA emission spectrum may be due to the
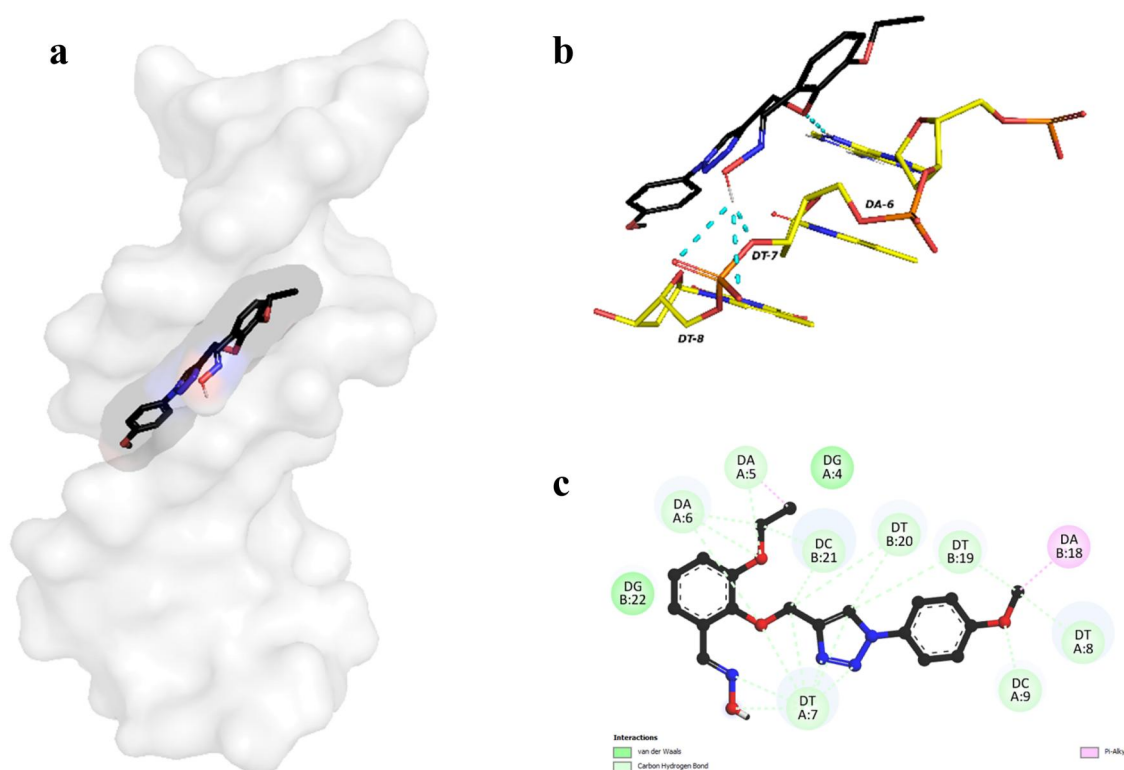
Figure 18. DNA-**3b** 3D (a), hydrogen bond interaction (**3b** black color stick, nucleotides yellow color stick and hydrogen bond turquoise color dashed line) (b) and 2D (c) binding position of the lowest binding affinity of **3b** at the active site of DNA.
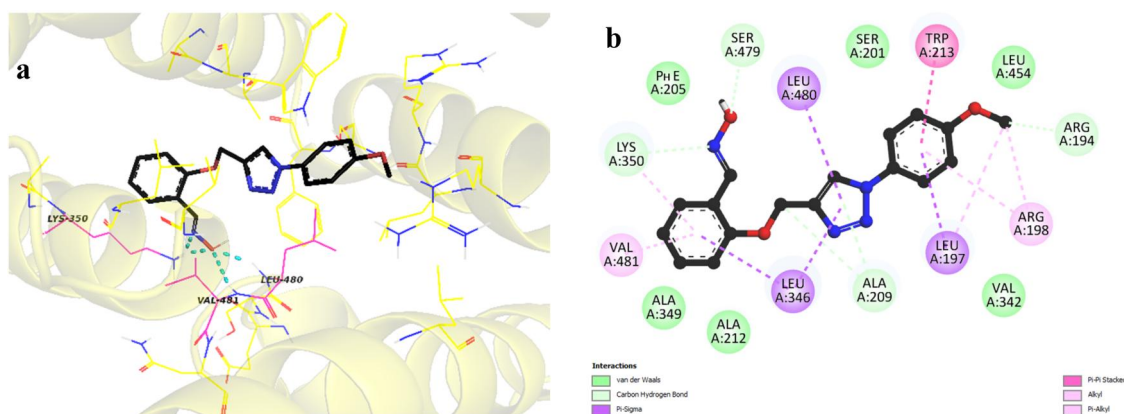

Figure 19. BSA-**1b** 3D (compound **1b** black color stick, pink color lines amino acids that form hydrogen bonds and hydrogen bond turquoise color dashed line) (a) and 2D (b) binding position of the lowest binding affinity at the subdomain IIA active site of BSA.

direct interaction of **3b** with Tyr213 (Attribution). The binding modes of other compounds are given in Figure S20 in Supplementary file.

Peripheral anionic region (PAS) (Tyr70 [72], Asp72 [74], Tyr121 [124], Trp279 [286] and Tyr334 [341]) are important amino acids located. PAS, located at the entrance to the active gate and including interaction with β-amyloid is responsible for extra activities (Şahin, Bingöl, Onur, Güngör, Köse, & Gülçin, 2022). The binding affinities of all compounds as a result of the AChE counter docking study, values ranging from (−10.17 kcal/mol) to (−9.41 kcal/mol) were presented in Table 4. According to these docking results, compound **3b** (−10.17 kcal/mol) showed stronger inhibitory activity than reference GNT (−9.37 kcal/mol) and other compounds. The most stable binding 2D and 3D pose of **3b**

were given in Figure 20. The oxime ($C = N$-OH) group of compound **3b** forms hydrogen bonds with Tyr334 (2.1 Å), ethoxy (OC_2H_5) group Ser 122 (2.1 Å) and methoxy (OCH_3) group Phe 288 (2.1 Å) residues. 1,2,3-Triazole ring of the compound, Tyr334 (3.97 Å) and Phe 330 (5.00 Å) amino acids made pi–pi stacking interactions. In addition, the compound makes van der Waals interaction with the important residues Asp72, Tyr121 and Tyr334 in the PAS region and the residues in the other active region. At the same time, experimental results revealed that compound **3b** showed the strongest inhibitory activity against AChE enzyme. Docking data indicated that it was a potent inhibitor of the AChE enzyme. The ethoxy group in **3b** structure makes both van der Waals and hydrophobic interactions. The binding modes of other compounds are given in Figure S21 in Supplementary file.
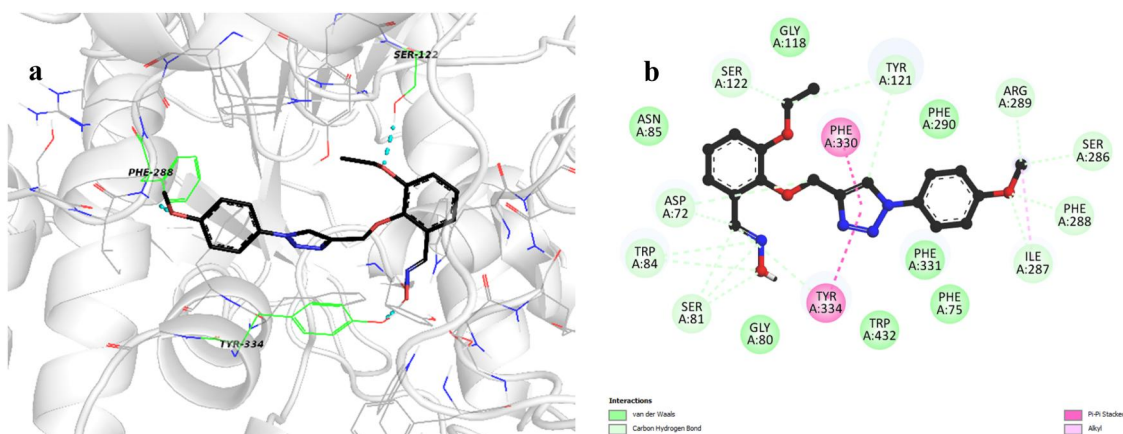
Figure 20. AChE-3b 3D (compound **3b** black color stick, green color lines amino acids that form hydrogen bonds and hydrogen bond turquoise color dashed line) (a) and 2D (b) binding position of the lowest binding affinity of **3b** at the active site of AChE.
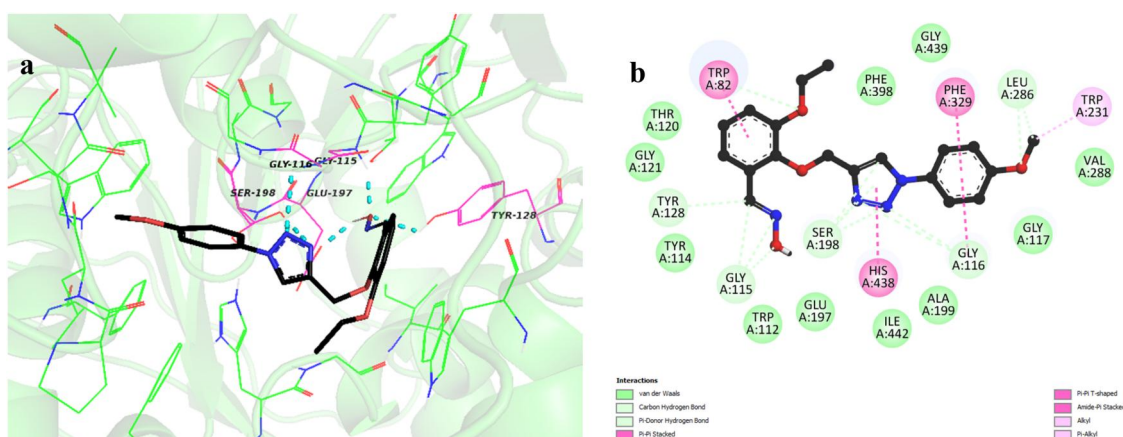

Figure 21. BChE-3b 3D (compound **3b** black color stick, pink color lines amino acids that form hydrogen bonds and hydrogen bond turquoise color dashed line) (a) and 2D (b) binding position of the lowest binding affinity of **3b** at the active site of BuChE.

BChE *versus* docking runs were performed to determine the interactions, binding modes and lowest binding energies of all compounds tested *in vitro* method. The binding energies of the compounds ranging from (−8.93 kcal/mol) to (−9.79 kcal/mol) as a result of docking were listed in Table 4. According to the docking results, **3b** (−9.79 kcal/mol) showed stronger inhibitory activity than reference THA (−7.77 kcal/mol) and other compounds. **3b** Binding modes and interaction types are given in Figure 21. Hetero atoms in the 1,2,3-triazole ring of **3b** hydrogen bonded with Ser198 (1.8 and 1.9 Å) and Tyr116 (2.6 Å) residues and the oxime group Gly115 (2.0 Å), Glu197 (1.8 Å) and Tyr128 (2.2 Å) with residues hydrogen bonded. Hetero atoms in the 1,2,3-triazole ring of **3b** were created hydrogen bonds with Ser198 (1.8 and 1.9 Å) and Tyr116 (2.6 Å) residues and the oxime group Gly115 (2.0 Å), Glu197 (1.8 Å) and Tyr128 (2.2 Å) residues. In addition, **3b** were formed pi–pi interactions Trp 82 (4.68 and 4.74 Å) with the oxime group, Phe 329 (5.98 Å) with the methoxy group and His 448 (4.42 Å) with the 1,2,3-triazole ring. In addition of many van der Waals and hydrophobic interactions were formed the most stable conformation of **3b** with the most basic binding orientations. Experimental and docking results are in harmony. The binding modes of other compounds are given in Figure S22 in Supplementary file.

4. Conclusion

In this article, we reported the synthesis of new 1,2,3-triazoles and their oxime derivatives. The synthesized compounds were accurately characterized using spectroscopic and analytical methods (FT–IR, ^{1}H/^{13}C NMR and elemental Analysis) studies. Crystal structures of compound **3**, **2b** and **3b** were elucidated by X-ray diffraction method. UV–vis absorption titration and fluorescence spectroscopy were used to determine the DNA binding affinity of the compounds. It was demonstrated by molecular docking studies that the oxime group -C=N-OH in the structure resulted in higher binding interaction with the DNA. Hyperchromism indicated that compounds **1a-3a** interact *via* non-covalent interaction with the DNA. These results were likewise confirmed by molecular docking studies. In addition, ethidium bromide displacement studies of compounds do not displace ethidium bromide, but they reduce the emission intensity by binding to other parts of the DNA chain. A conformational change in the Trp-212 microenvironments located in subdomain IIA of the plasma protein is evident from the results of the BSA binding titration. The values of the BSA binding constants indicate a moderate binding of **3b** to the BSA. The binding of the compounds with BSA is desired for transporting the compound into the DNA region. Compounds

synthesized as another biological activity were screened for their potential to inhibit the activities of AChE and BuChE enzymes. It was observed that all synthesized compounds had higher enzyme activities except **1a–3a**. Among the 1,2,3-triazole oxime derivatives, it was observed that **3b** had a higher activity against AChE ($IC_{50} = 4.8\ \mu M$) and BuChE ($IC_{50} = 70.16\ \mu M$). We concluded that the reason for this was that the ethyl part of the structure was even more effective in inhibiting the enzyme. Compounds **2b** and **3b**, which are oxime in their structure, were found to be approximately twice as active for AChE when compared to the standard component GNT. Compounds **2b** and **3b** with the best activity were subjected to kinetic studies and Ki values of **2b** and **3b** were 3.50 ± 0.21 and 2.10 ± 0.35 μM, respectively. These results suggest that **2b** and **3b** are potent non-competitive inhibitors for AChE. It also shows that it has a complex inhibition mechanism. Molecular docking studies have confirmed the experimental results.

Acknowledgements

Disclosure statement

The authors declare that they have no conflict of interest.

Funding

ORCID

Seyit Ali Gungor (iD) http://orcid.org/0000-0002-3233-4529

Data availability statement

The data that support the findings of this study are available in the supplementary material of this article. Data will be made available on request.

References

Abdel-Aziz, M., Abuo-Rahma, G. E. D. A. A., Beshr, E. A. M., & Ali, T. F. S. (2013). New nitric oxide donating 1,2,4-triazole/oxime hybrids: Synthesis, investigation of anti-inflammatory, ulceroginic liability and antiproliferative activities. *Bioorganic & Medicinal Chemistry*, 21(13), 3839–3849. https://doi.org/10.1016/j.bmc.2013.04.022

Abdel-Wahab, B. F., Abdel-Latif, E., Mohamed, H. A., & Awad, G. E. A. (2012). Design and synthesis of new 4-pyrazolin-3-yl-1,2,3-triazoles and 1,2,3-triazol-4-yl-pyrazolin-1-ylthiazoles as potential antimicrobial agents. *European Journal of Medicinal Chemistry*, 52, 263–268. https://doi.org/10.1016/j.ejmech.2012.03.023

Abele, E., Abele, R., Rubina, K., & Lukevics, E. (2005). Quinoline oximes: Synthesis, reactions, and biological activity. *Chemistry of Heterocyclic Compounds*, 41(2), 137–162. https://doi.org/10.1007/s10593-005-0119-2

Abele, E., & Lukevics, E. (2010). ChemInform abstract: Furan and thiophene oximes: Synthesis, reactions, and biological activity. *ChemInform*, 32(46), 141-169. https://doi.org/10.1002/chin.200146276

Aleksić, M. M., & Kapetanović, V. (2014). An overview of the optical and electrochemical methods for detection of DNA - drug interactions. *Acta Chimica Slovenica*, 61(3), 555–573.

Botta, C. B., Cabri, W., Cini, E., De Cesare, L., Fattorusso, C., Giannini, G., Persico, M., Petrella, A., Rondinelli, F., Rodriquez, M., Russo, A., & Taddei, M. (2011). Oxime amides as a novel zinc binding group in histone deacetylase inhibitors: Synthesis, biological activity, and computational evaluation. *Journal of Medicinal Chemistry*, 54(7), 2165–2182. https://doi.org/10.1021/jm101373a

Butour, J., & Macquet, J. (1981). Viscosity, nicking, thermal and alkaline denaturation studies on three classes of dna-platinum complex. *Biochimica Et Biophysica Acta*, 653(3), 305–315. https://doi.org/10.1016/0005-2787(81)90187-8

Chowdhury, M. H., Aslan, K., Malyn, S. N., Lakowicz, J. R., & Geddes, C. D. (2006). Metal-enhanced chemiluminescence. *Journal of Fluorescence*, 16(3), 295–299. https://doi.org/10.1007/s10895-006-0082-z

Çot, A., Çeşme, M., Onur, S., Aksakal, E., Şahin, İ., & Tümer, F. (2023). Rational design of 1,2,3-triazole hybrid structures as novel anticancer agents: Synthesis, biological evaluation and molecular docking studies. *Journal of Biomolecular Structure & Dynamics*, 41(14), 6857–6865. https://doi.org/10.1080/07391102.2022.2112620

El-Ghiaty, M. A., Alqahtani, M. A., & El-Kadi, A. O. S. (2023). Chemico-Biological Interactions Modulation of cytochrome P450 1A (CYP1A) enzymes by monomethylmonothioarsonic acid (MMMTA V) in vivo and in vitro. *Chemico-Biological İnteractions*, 376, 110447. https://doi.org/10.1016/j.cbi.2023.110447

Feizi-Dehnayebi, M., Dehghanian, E., & Mansouri-Torshizi, H. (2021). Spectrochimica Acta Part A : Molecular and Biomolecular Spectroscopy A novel palladium (II) antitumor agent : Synthesis, characterization, DFT perspective, CT-DNA and BSA interaction studies via in-vitro and in-silico approaches. *Spectrochimica Acta Part A, Molecular and Biomolecular Spectroscopy*, 249, 119215. https://doi.org/10.1016/j.saa.2020.119215

Feizi-Dehnayebi, M., Dehghanian, E., & Mansouri-Torshizi, H. (2022). Biological activity of bis-(morpholineacetato)palladium(II) complex: Preparation, structural elucidation, cytotoxicity, DNA-/serum albumin-interaction, density functional theory, in-silico prediction and molecular modeling. *Spectrochimica Acta Part A, Molecular and Biomolecular Spectroscopy*, 281, 121543. https://doi.org/10.1016/j.saa.2022.121543

Francis, P. T., Palmer, A. M., Snape, M., & Wilcock, G. K. (1999). The cholinergic hypothesis of Alzheimer's disease: A review of progress. *Journal of Neurology, Neurosurgery, and Psychiatry*, 66(2), 137–147. https://doi.org/10.1136/jnnp.66.2.137

Galindo-Murillo, R., Garc, J. C., Ruiz-Azuara, L., Cheatham, E., & Cort, F. (2015). Intercalation processes of copper complexes in DNA. *Nucleic Acids Research*, 43(11), 5364–5376. https://doi.org/10.1093/nar/gkv467

Giannousi, K., Geromichalos, G., Kakolyri, D., Mourdikoudis, S., & Dendrinou-Samara, C. (2020). The interaction of ZnO nanostructures with proteins : In vitro fibrillation/antifibrillation studies and in silico molecular docking simulations. *ACS Chemical Neuroscience*, 11(3), 436–444. https://doi.org/10.1021/acschemneuro.9b00642

Güngör, S. A., Köse, M., Tümer, M., & Bal, M. (2021). Structural characterization, DNA binding properties and molecular docking studies of imine compounds derived from Disperse black 9. *Journal of Molecular Structure*, 1243, 130776. https://doi.org/10.1016/j.molstruc.2021.130776

Gungor, O., & Kose, M. (2023). The biguanide–sulfonamide derivatives: Synthesis, characterization and investigation of anticholinesterase inhibitory, antioxidant and DNA/BSA binding properties. *Journal of Biomolecular Structure & Dynamics*, 0(0), 1–16. https://doi.org/10.1080/07391102.2023.2184637

Güngör, S. A., Köse, M., Tümer, M., Türkeş, C., & Beydemir, Ş. (2022). Synthesis, characterization and docking studies of benzenesulfonamide derivatives containing 1,2,3-triazole as potential ınhibitor of carbonic anhydrase I-II enzymes. *Journal of Biomolecular Structure & Dynamics*, 41(20), 10919–10929. https://doi.org/10.1080/07391102.2022.2159531

Knappe, G. A., Wamhoff, E. C., & Bathe, M. (2023). Functionalizing DNA origami to investigate and interact with biological systems. *Nature Reviews Materials*, 8(2), 123–138. https://doi.org/10.1038/s41578-022-00517-x

Kose, R., Gungor, S. A., Erkan Kariper, S., Kose, M., & Kurtoglu, M. (2017). The new O,O and N,O type ligands and their Cu(II) and Ni(II) complexes: Crystal structure, absorption-emission properties and superoxide dismutase mimetic studies. *Inorganica Chimica Acta*, 462, 130–141. https://doi.org/10.1016/j.ica.2017.03.022

Kumar, V., Saha, A., & Roy, K. (2020). In silico modeling for dual inhibition of acetylcholinesterase (AChE) and butyrylcholinesterase (BuChE) enzymes in Alzheimer's disease. *Computational Biology and Chemistry*, 88, 107355. https://doi.org/10.1016/j.compbiolchem.2020.107355

Li, X., Lin, Y., Yuan, Y., Liu, K., & Qian, X. (2011). Novel efficient anticancer agents and DNA-intercalators of 1,2,3-triazol-1,8-naphthalimides: Design, synthesis, and biological activity. *Tetrahedron*, 67(12), 2299–2304. https://doi.org/10.1016/j.tet.2011.01.063

Links, D. A., Raja, D. S., Bhuvanesh, N. S. P., & Natarajan, K. (2012). PAPER A novel water soluble ligand bridged cobalt(II) coordination polymer of 2-oxo-1,2-dihydroquinoline-3-carbaldehyde (isonicotinic) hydrazone: Evaluation of the DNA binding, protein interaction, radical scavenging and anticancer activity. *Dalton Transactions*, 41(15), 4365–4377. https://doi.org/10.1039/c2dt12274j

Najafi, Z., Mahdavi, M., Saeedi, M., Karimpour-Razkenari, E., Asatouri, R., Vafadarnejad, F., Moghadam, F. H., Khanavi, M., Sharifzadeh, M., & Akbarzadeh, T. (2017). Novel tacrine-1,2,3-triazole hybrids: In Vitro, in vivo biological evaluation and docking study of cholinesterase inhibitors. *European Journal of Medicinal Chemistry*, 125, 1200–1212. https://doi.org/10.1016/j.ejmech.2016.11.008

Pala, N., Esposito, F., Rogolino, D., Carcelli, M., Sanna, V., Palomba, M., Naesens, L., Corona, A., Grandi, N., Tramontano, E., & Sechi, M. (2016). Inhibitory effect of 2,3,5,6-tetrafluoro-4-[4-(Aryl)-1H-1,2,3-triazol-1-yl]benzenesulfonamide derivatives on HIV reverse transcriptase associated RNase H activities. *International Journal of Molecular Sciences*, 17(8), 1371. https://doi.org/10.3390/ijms17081371

Rakesh, K. P., Kumara, H. K., Manukumar, H. M., & Channe Gowda, D. (2019). Anticancer and DNA binding studies of potential amino acids based quinazolinone analogs: Synthesis, SAR and molecular docking. *Bioorganic Chemistry*, 87, 252–264. https://doi.org/10.1016/j.bioorg.2019.03.038

Ray, A., Seth, B. K., Pal, U., & Basu, S. (2012). Spectrochimica acta part A: Molecular and Biomolecular Spectroscopy Nickel (II) -Schiff base complex recognizing domain II of bovine and human serum albumin: Spectroscopic and docking studies. *Spectrochimica Acta Part A, Molecular and Biomolecular Spectroscopy*, 92, 164–174. https://doi.org/10.1016/j.saa.2012.02.060

Şahin, İ., Bingöl, Z., Onur, S., Güngör, A., Köse, M., & Gülçin, İ. (2022). Enzyme inhibition properties and molecular docking studies of 4-sulfonate containing aryl α-hydroxyphosphonates based hybrid. *Chemistry & Biodiversity*, 19, e202100787. https://doi.org/10.1002/cbdv.202100787

Şahin, İ., Bingöl, Z., Onur, S., Güngör, S. A., Köse, M., Gülçin, İ., & Tümer, F. (2022). Enzyme inhibition properties and molecular docking studies of 4-sulfonate containing Aryl α-hydroxyphosphonates based hybrid molecules. *Chemistry & Biodiversity*, 19(5), e202100787. https://doi.org/10.1002/cbdv.202100787

Şahin, İ., Özgeriş, F. B., Köse, M., Bakan, E., & Tümer, F. (2021). Synthesis, characterization, and antioxidant and anticancer activity of 1,4dDisubstituted 1,2,3-triazoles. *Journal of Molecular Structure*, 1232, 130042. https://doi.org/10.1016/j.molstruc.2021.130042

Suh, D., & Chaires, J. B. (1995). *Criteria for the Mode of Binding of DNA Binding Agents*, Bioorganic & medicinal chemistry, 3(6), 723–728. https://doi.org/10.1016/0968-0896(95)00053-J

Tian, F. F., Jiang, F. L., Han, X. L., Xiang, C., Ge, Y. S., Li, J. H., Zhang, Y., Li, R., Ding, X. L., & Liu, Y. (2010). Synthesis of a novel hydrazone derivative and biophysical studies of its interactions with bovine serum albumin by spectroscopic, electrochemical, and molecular docking methods. *The Journal of Physical Chemistry. B*, 114(46), 14842–14853. https://doi.org/10.1021/jp105766n

Toneatto, J., & Argüello, G. A. (2011). New advances in the study on the interaction of [Cr (phen) 2 (dppz)] 3 + complex with biological models; association to transporting proteins. *Journal of İnorganic Biochemistry*, 105(5), 645–651. https://doi.org/10.1016/j.jinorgbio.2010.10.018

Vecchio, I., Sorrentino, L., Paoletti, A., Marra, R., & Arbitrio, M. (2021). The state of the art on acetylcholinesterase inhibitors in the treatment of Alzheimer's disease. *Journal of Central Nervous System Disease*, 13, 11795735211029113. https://doi.org/10.1177/11795735211029113

Venugopala, K. N., Rao, G. B. D., Bhandary, S., Pillay, M., Chopra, D., Aldhubiab, B. E., Attimarad, M., Alwassil, O. I., Harsha, S., & Mlisana, K. (2016). Design, synthesis, and characterization of (1-(4-aryl)1h-1,2,3-triazol-4-yl)methyl, substituted phenyl6-methyl-2-oxo-1,2,3,4-tetrahydropyrimidine-5carboxylates against Mycobacterium tuberculosis. *Drug Design, Development and Therapy*, 10, 2681–2690. https://doi.org/10.2147/DDDT.S109760

Ware, R. (1962). *Oxygek Qcexchıkg of Fluorescence in Eolftiov*, 1, 1949–1952.

Weng, Y., Huang, Q., Li, C., Yang, Y., Wang, X., Yu, J., Huang, Y., & Liang, X. J. (2020). Improved nucleic acid therapy with advanced nanoscale biotechnology. *Molecular Therapy Nucleic Acids*, 19, 581–601. https://doi.org/10.1016/j.omtn.2019.12.004

Yadav, P., Lal, K., Rani, P., Mor, S., Kumar, A., & Kumar, A. (2017). Efficient synthesis and antimicrobial evaluation of 2-((1-substituted-1H-1,2,3-triazol-4-yl)-1-naphthaldehydes and their oxime derivatives. *Medicinal Chemistry Research*, 26(7), 1469–1480. https://doi.org/10.1007/s00044-017-1845-6

Zhang, X., Li, S., Yang, L., & Fan, C. (2007). Synthesis, characterization of Ag (I), Pd (II) and Pt (II) complexes of a triazine-3-thione and their interactions with bovine serum albumin. *Spectrochimica Acta Part A, Molecular and Biomolecular Spectroscopy*, 68(3), 763–770. https://doi.org/10.1016/j.saa.2006.12.058